NASA TECHNICAL NOTE

NASA TN D-2827

c. 1

NASA TN D-2827

STUDY OF THE STABILITY AND DRAG AT MACH NUMBERS FROM 4.5 TO 13.5 OF A CONICAL VENUS-ENTRY BODY

by Peter F. Intrieri

Ames Research Center
Moffett Field, Calif.

NATIONAL AERONAUTICS AND SPACE ADMINISTRATION • WASHINGTON, D. C. • MAY 1965

NASA TN D-2827

STUDY OF THE STABILITY AND DRAG AT MACH NUMBERS FROM 4.5 TO 13.5 OF A CONICAL VENUS-ENTRY BODY

By Peter F. Intrieri

Ames Research Center
Moffett Field, Calif.

NATIONAL AERONAUTICS AND SPACE ADMINISTRATION

For sale by the Clearinghouse for Federal Scientific and Technical Information
Springfield, Virginia 22151 – Price $2.00

STUDY OF THE STABILITY AND DRAG AT MACH NUMBERS FROM 4.5 TO 13.5 OF A CONICAL VENUS-ENTRY BODY

By Peter F. Intrieri
Ames Research Center

SUMMARY

An experimental study has been conducted to determine the static and dynamic stability and drag characteristics of a conical-nosed planetary-entry vehicle in a gas mixture composed of 9-percent carbon dioxide and 91-percent nitrogen and in air at Mach numbers of 4.5, 9.0, and 13.5 and Reynolds numbers from 0.4 to 1.2 million. It was determined that for the assumed center-of-gravity location, the configuration is statically and dynamically stable at all Mach numbers and throughout the angle-of-attack range of the investigation and that it exhibits the same static stability, dynamic stability, and drag in air as it does in the nitrogen--carbon-dioxide mixture. The static stability is invariant with Mach number and nonlinear with angle of attack. The nonlinear variation of pitching moment with angle of attack was closely approximated by a two-term power series of the resultant angle of attack. The dynamic stability is invariant with Mach number and angle of attack. The drag coefficient of the configuration is essentially invariant with Mach number and increases with increasing angle of attack. The static stability and drag were closely predicted by Newtonian theory.

Strong experimental evidence is presented which shows that the configuration is statically stable only about a nose-forward trim attitude of zero angle of attack and dynamically stable about this unique stable attitude for all amplitudes of oscillation.

Calculations which use the measured stability results to describe the oscillatory behavior of a full-scale vehicle flying an example entry trajectory through a model of the Venus atmosphere indicate that the stability characteristics of the present configuration should be adequate for orienting the vehicle properly during a Venus entry. For all initial orientations of the vehicle (nose forward or base forward) the pitching motions should converge to a very small fraction of the amplitude at entry.

INTRODUCTION

In the design of vehicles intended to enter planetary atmospheres, two important goals are to provide for minimum aerodynamic heating and for adequate aerodynamic stability of the vehicle during entry. For entries into the Earth's atmosphere at velocities well in excess of escape velocity, reference 1 has shown that the total heating will be less for sharp entry bodies, such as pointed cones, than for blunt bodies. Radiative heating which becomes the dominant mode at these speeds depends on the velocity normal to the bow-shock wave rather than on the free-stream velocity; therefore, the combined radiative and convective heating will be drastically reduced if the entry bodies have highly swept bow-shock waves. Reference 2 indicates that in the nitrogen--carbon-dioxide atmospheres of Venus and Mars, the radiative intensities will be significantly greater than in air. The advantages of using conical entry bodies to reduce total heating in these atmospheres are shown by the analysis of reference 3.

Having established the desirability of conical shapes from heating considerations, it must be ascertained, for a passive system, that the stability of such vehicles flying in the N_2-CO_2 atmospheres will be adequate to insure proper orientation of its heat shield during the entry, and, in particular, that the vehicle's dynamic stability will be sufficient to prevent divergent oscillations which could result in a mission failure. Also, since the constituents of the planetary atmospheres through which these vehicles must descend are known only within certain limits (see, e.g., ref. 4), it is important to determine whether the aerodynamic characteristics of the vehicle are sensitive to changes in gas composition and whether these characteristics can be predicted satisfactorily.

The static and dynamic stability and drag characteristics of a conical configuration were investigated in the prototype of the Ames Hypervelocity Free-Flight Facility at nominal Mach numbers of 4.5, 9.0, and 13.5 and at Reynolds numbers of 0.4, 0.8, and 1.2 million, respectively, based on free-stream conditions and model diameter. The models were tested in a gas mixture composed of 9-percent carbon dioxide and 91-percent nitrogen (by volume) and also in air. Two exploratory flights were also made with the models launched backward to determine whether they would remain flying backward or, as expected from calculations, would begin righting themselves to a nose-forward attitude. Theoretical estimates of static stability and drag were made and compared with the experimental results.

SYMBOLS

A	reference area, maximum body cross-sectional area, meters^2
C_1	arbitrary constant in equation (10)
C_D	drag coefficient, $\dfrac{\text{total drag}}{q_\infty A}$, dimensionless
C_{D_o}	drag coefficient at zero angle of attack
C_L	lift coefficient, $\dfrac{\text{lift}}{q_\infty A}$, dimensionless
C_{L_α}	lift-curve slope, per radian

C_m	pitching-moment coefficient, $\frac{\text{pitching moment}}{q_\infty Ad}$, dimensionless
C_{m_α}	pitching-moment-curve slope, per radian
$C_{m_q} + C_{m_{\dot{\alpha}}}$	damping-in-pitch derivative, $\frac{\partial C_m}{\partial(qd/V)} + \frac{\partial C_m}{\partial(\dot{\alpha}d/V)}$, per radian
d	reference diameter, maximum body diameter, cm
g	average gravitational acceleration within the atmosphere of a planet, m/sec^2
h	altitude above planet surface, km
I_y	moment of inertia about a transverse axis through the center of gravity, $kg\text{-}m^2$
k	constant in equation (1)
K	dynamic-stability parameter for variable density (eq. (11)), dimensionless
K_1,K_2,K_3	constants in equation (2), deg
m	mass of model, gm
M	Mach number, dimensionless
M_n	restoring-moment coefficients, defined by equation (A1)
$M_0,\ldots,M_6$	restoring-moment coefficients, defined by equation (A4)
n	integer denoting number of complete tumbles of vehicle
p	roll parameter, roll rate/velocity, radians/m
P	static pressure, $newtons/m^2$
q	angular pitching velocity, radians/sec
q_∞	free-stream dynamic pressure, $newtons/m^2$
R	gas constant for atmospheric gas mixture, $\frac{P}{\rho T}$, $m^2/sec^2\ {}^oK$
Re	Reynolds number based on free-stream gas properties and maximum diameter, dimensionless
t	time

T	gas temperature, $^{\circ}K$
u	horizontal component of flight velocity, m/sec
V	velocity along flight path, m/sec
x	distance along flight path, m
x_{cg}	axial distance from model nose to center-of-gravity position, cm
y	horizontal coordinate normal to the flight path, m
z	coordinate normal to the flight path and y axis, m
α	angle of attack (angle between model axis and resultant wind direction projected onto the vertical plane), deg
β	angle of sideslip (angle between model axis and resultant wind direction projected onto the horizontal plane), deg
β_V	reciprocal of atmospheric scale height, $\frac{g}{RT}$, per m
γ	flight-path angle (referenced to the local horizontal), deg
ϵ	dependent variable, $-\frac{\alpha}{2} + n\pi$, deg
ϵ_p	value of ϵ at the first peak of oscillatory motion
η_1,η_2	damping exponents in equation (2), m^{-1}
θ,ψ	attitude coordinates of the model relative to Earth-fixed axis, deg
λ	wave length of pitching oscillation, m/cycle
ξ	dynamic-stability parameter for constant altitude (eq. (5)), dimensionless
ρ	atmospheric density, kg/m^3
σ	resultant angle of attack, $\tan^{-1}\sqrt{\tan^2\alpha + \tan^2\beta}$, deg, or transverse radius of gyration, $\frac{I_y}{x}$, when used in parameter $\left(\frac{d}{\sigma}\right)^2$ in equations (5), (8), and (11) and in table I, m
σ_m	maximum resultant angle of attack, deg
σ_o	minimum resultant angle of attack, deg
σ_{rms}	root-mean-square resultant angle of attack, $\sqrt{\frac{\int_0^x \sigma^2}{x} dx}$, deg
ω	frequency, radians/sec

ω_1, ω_2 rate of rotation of complex vectors which generate the model pitching motion (eq. (2)), radians/m

$(\dot{\ })$ first derivative with respect to time

$(\ddot{\ })$ second derivative with respect to time

Subscripts

cg center of gravity

env envelope

i initial condition

max maximum

min minimum

o conditions at surface of planet

∞ free-stream conditions

CONFIGURATION

The configuration selected had a 30° half-angle cone forebody. This forebody, as is shown in references 1 and 3, is close to the optimum cone angle for minimizing total heating at velocities well above escape velocity. The afterbody geometry was selected by the requirement that the configuration be stable only with the 30° half-angle cone pointed forward. This requirement was fulfilled by the addition of a short cylinder and a rearward pointing cone to the base of the forebody. The cylinder length of 0.125 model diameter and the rearward pointing cone half-angle of 48° were selected to provide a coincident center-of-pressure location for both base-forward and nose-forward flight of the vehicle and also to provide useful volume. Figure 1(a) is a sketch of a model of this configuration, giving pertinent nominal dimensions.

DESCRIPTION OF TESTS

Test Technique and Test Conditions

The tests were performed in the prototype of the Ames Hypervelocity Free-Flight Facility by launching models from a deformable-piston, light-gas gun of 12.7 mm bore (ref. 5) into a quiescent mixture composed of 9-percent carbon dioxide and 91-percent nitrogen (by volume), and into still air at ambient temperature. Nominal model velocities of 1.52, 3.05, and 4.72 km/sec were obtained corresponding to nominal Mach numbers of 4.5, 9.0, and 13.5, respectively. In order to obtain adequate definition of the motions of the models through the test section, with the given spacing of shadowgraph stations (see below), the ambient test-section pressure was set at 4×10^4 newtons/m^2 (300 mm of mercury), to give the desired wave length of oscillation. Corresponding Reynolds numbers are shown in table I, which lists the average values of Mach number, Reynolds number, and test gas for each flight. Gas samples taken immediately prior to each firing in the N_2-CO_2 mixture were analyzed for chemical content on a mass spectrograph and were found to contain the desired concentration of CO_2 and N_2 within 1 percent, with only trace amounts of other constituents.

The trajectory of the model through the test section was recorded by 11 spark shadowgraph stations located at 1.22-meter intervals. Side and top views of the models were recorded at each station. The shadowgraphs contained images of reference wires from which x,y,z,θ, and ψ coordinates were read. The linear coordinates were measured to within 0.0076 cm, and the angles to within 0.25°. The orientation angles θ and ψ were read relative to Earth-fixed axes. No corrections were made for the angle between the resultant wind direction and Earth-fixed axes to give values of α and β since, for these tests, these corrections were within the reading accuracy of the angles θ and ψ. Time of model flight between stations was recorded with electronic chronographs to within 0.05 microsecond (0.02 percent of the time of flight between stations of a model flying at 4.72 km/sec).

Models and Sabots

Sketches of the two types of models used in the present investigation, showing pertinent nominal dimensions, are presented in figure 1. The after-sections of the models shown in figure 1(a) were machined from 7075-T6 aluminum; the front sections of the models were machined from a tungsten-iron alloy (Mallory 3000) to obtain a center-of-gravity location of 0.72 d from the nose. These models were used in the tests at Mach numbers of 4.5 and 9.0. However, at the highest Mach number ($M = 13.5$), the heating rates encountered were sufficiently high to cause the models to burn in flight. It was found that a thin plastic coating over the models provided a successful heat shield. The coating consisted of a polymer of vinylidene fluoride sprayed onto the model surface to a thickness of about 0.04 cm. The models were remachined and trimmed to give a final coat thickness of about 0.019 cm. Figure 1(b) is a sketch of the coated models showing pertinent nominal dimensions. The after-sections of these plastic-coated models were machined from a titanium alloy since the heat-curing of the plastic was found to anneal the aluminum after-section so that it deformed severely during the launch. The strength of the titanium alloy was not affected by the curing. Since titanium is heavier than aluminum, the size of the Mallory front section was adjusted (see fig. 1(b)) so that the center-of-gravity location of these models, prior to being coated, was the same as that for the basic models - 0.72 d from the nose. The amount, and consequently the weight distribution, of the plastic used in the coating was small; therefore, the location of the center of gravity relative to any point on the metal model did not change. However, the distance of the center of gravity to the new plastic nose of the coated model was increased by the length of plastic deposited at the nose - approximately 0.038 cm. Examination of the shadowgraph pictures (fig. 2) of two of these models in flight at Mach number 13.5 shows that although ablation of the plastic occurred during the flights, any change in shape, particularly blunting of the tip, was insignificant. The position of the center of gravity for all the models was measured within ±0.0025 cm accuracy. The dimensions of the models varied only slightly from those shown in figure 1. Some of the measured physical characteristics of each model are listed in table I.

Photographs of the models and sabots are presented in figure 3. Three different sabot types were used in launching the models: a straight sabot (fig. 3(a)) for flights at angles of attack below 10°, a canted sabot (fig. 3(b)) for flights at angles of attack as high as 45°, and a sabot for launching the models in the base-forward attitude (fig. 3(d)). The canted sabot was not always successful in producing high angle-of-attack flights and, as can be seen in table I, resulted in a large number of low angle-of-attack flights in the N_2-CO_2 mixture. Tests using the canted sabot to launch the coated models at a Mach number of 13.5 were unsuccessful because the models broke up inside the gun. The straight sabot was successful in obtaining low-angle flights at this Mach number. The sabots were machined from Lexan polycarbonate plastic.

REDUCTION OF DATA

Drag

The determination of drag coefficient from the time-distance data was based on the procedure described in reference 6, in which a constant drag coefficient is assumed. A procedure applicable to cases where the drag coefficient varies with angle of attack is presented in reference 7. It is shown in this reference that if the drag coefficient varies with the square of the local resultant angle of attack, according to the relation

$$C_D = C_{D_o} + k\sigma^2 \tag{1}$$

the drag coefficient obtained by the method of reference 6, under certain additional constraints, is the drag coefficient that would be obtained in steady flight at a resultant angle of attack equal to the root-mean-square resultant angle of attack, σ_{rms}. Accordingly, the present results are correlated with σ_{rms}.

Stability Derivatives

The pitching and yawing motions of the models during free flight were analyzed to determine the stability derivatives. Examples of the types of motions encountered in the present tests, as viewed in the α-β plane, are shown in figure 4. The angles of attack and sideslip measured from the shadowgraphs at each station are indicated by the symbols. The curves show the theoretical motions which best fit the experimental data and were computed by a method which will be discussed later in this section. Since the models are aerodynamically symmetric, the angular displacement of the model, at any instant, can be represented also by the resultant angle of attack, σ, whose orthogonal components are the angles α and β. It can be seen in figure 4 that, in general, the data show precessing elliptical motions, and that the angle range through which the models oscillate differs for each flight. Also, it should be noted that the models in the tests at Mach numbers of 4.5 and 9.0 underwent two complete cycles of oscillation (figs. 4(a), (b), (c), and (d)), whereas the models in the tests at Mach number of 13.5, because they were heavier (see discussion under Models and Sabots), underwent only one and one-half cycles of oscillation (figs. 4(e) and (f)). Although one and one-half cycles of motion are usually sufficient to define the desired stability derivatives, more cycles of well-defined motion will generally produce better data.

Stability derivatives were obtained from analysis of the pitching and yawing motions of the models. For each flight, the measured variation of α and β with x was represented by the following equation:

$$\beta + i\alpha = K_1 e^{(\eta_1 + i\omega_1)x} + K_2 e^{(\eta_2 - i\omega_2)x} + K_3 e^{ipx} \tag{2}$$

Equation (2) is the solution of the linear differential equation of motion, as given in reference 8, and includes effects of model spin and trim angle on the motion. Some of the basic assumptions used in the development of this equation are: axially symmetric configuration, linear variations of force and moment with angle of attack, small angular displacements, and small angles of trim. Equation (2) programed for machine computation (ref. 9) was used to select optimum values of all the constants by an iterative process of differential corrections. The curves shown in figure 4 were obtained by fitting equation (2) to the experimental data. The closeness of the computed curves to the experimental data is a measure of the reliability of the stability results. The fitted curves for all the flights analyzed in this investigation agreed with the measured angles within the measuring accuracy.

The pitching-moment-curve slope, C_{m_α}, was computed from the wave length of oscillation by means of

$$-C_{m_\alpha} = \frac{8\pi^2 I_y}{\lambda^2 \rho A d} \tag{3}$$

where

$$\lambda = \frac{2\pi}{\sqrt{\omega_1 \omega_2}} \tag{4}$$

The dynamic-stability parameter, ξ, defined as

$$\xi = C_D - C_{L_\alpha} + (C_{m_q} + C_{m_{\dot\alpha}})\left(\frac{d}{\sigma}\right)^2 \tag{5}$$

was determined from the constants η_1 and η_2 by means of the relation

$$\eta_1 + \eta_2 = \frac{\rho A}{2m} \xi \tag{6}$$

It has been shown in references 9 and 10 that ξ, in the form shown in equation (5), is a convenient parameter for describing the dynamic stability of an unpowered vehicle in free flight at constant altitude. The values of ξ, presented in this report, were obtained from equations (2) and (6) which assume a linear system over the angle-of-attack range covered during any one flight. Each value of ξ, therefore, is the dynamic-stability parameter of an equivalent linear system whose amplitude of oscillation would grow or diminish in the same way as that experienced by the model.

RESULTS AND DISCUSSION

The experimental results of this investigation define the drag, static-stability, and dynamic-stability characteristics of the configuration in the angle-of-attack range from 0° to 40°, at Mach numbers of 4.5, 9.0, and 13.5, in a gas mixture composed of 9-percent carbon dioxide and 91-percent nitrogen and also in air. The measured values of C_D, C_{m_α}, and ξ, obtained from analysis of 65 separate model flights, are summarized in table I. These coefficients are based on the maximum model diameter and frontal area. Values of σ_m, σ_o, and σ_{rms} presented in table I indicate the angle-of-attack range through which each model oscillated during the flight. Full-scale enthalpy values were duplicated in these tests and, as stated earlier, at the highest Mach number (13.5), the heating rates were sufficiently high to cause ablation of the protective plastic coating on the models. These models survived the flights without significant change in surface shape. The effects of gas dissociation and surface ablation cannot be isolated but are implicit in the experimental results. Shadowgraphs, typical of those obtained in the present tests, are presented in figures 5 and 6 to illustrate gross features of the flow fields, particularly the bow-shock wave. Theoretical estimates of static stability and drag made using conical flow theory (ref. 11), and the equations developed in reference 12, based on Newtonian impact theory, are compared with the experimental results.

Drag Characteristics

The measured values of drag coefficient presented as a function of the root-mean-square resultant angle of attack in figure 7 show that the drag coefficient increases approximately 30 percent as the angle of attack is increased from 0° to 28°. These data also show that in this angle-of-attack range the configuration exhibits the same drag characteristics in air as it does in the carbon dioxide and nitrogen mixture. The drag coefficient is seen to decrease slightly (approximately 8 percent) as the Mach number is increased from 4.5 to 9.0 but is seen to remain constant, within the scatter of the data, for a further increase in Mach number to 13.5. Comparison of the experimental results with values calculated for zero angle of attack using conical-flow theory shows that although the theory is in excellent agreement with the experimental data at Mach numbers 9.0 and 13.5, and predicts the correct trend with Mach number, the theory underestimates the drag at Mach number 4.5 by about 6.5 percent. Estimates were made of the base-pressure contribution to the drag for all three Mach numbers using a Prandtl-Meyer expansion around the base of the model and flow deflection angles measured from shadowgraphs similar to those presented in figures 5 and 6. These estimates if applied would raise the theoretical values at Mach numbers 4.5, 9.0, and 13.5 by about 6.5, 1.5, and 1 percent of the measured values, respectively, and would result in excellent agreement with the experimental results. The effect of angle of attack on drag is well predicted by Newtonian flow theory.

Static-Stability Characteristics

The experimental values of the equivalent linear pitching-moment-curve slope, C_{m_α}, are presented in figure 8 as a function of the maximum resultant angle of attack, σ_m. For a nonlinear system the stability results, unlike the drag results, do not correlate with σ_{rms} so are presented as functions of σ_m, which is convenient for the further analysis of the data by nonlinear methods. The data have been corrected for the variations in center-of-gravity location shown in table I to a common center-of-gravity position, 0.72 d from the nose. With the exception of flight number 853 (see table I), these corrections to the data of Mach number of 4.5 and 9.0 were small, usually within 4 percent (the measuring accuracy of center-of-gravity position). However, the corrections to the data of Mach number 13.5 were on the order of 20 percent, since, as discussed earlier, at this Mach number the models required a protective plastic coating which caused their centers of gravity to be at 0.733 d from the nose (see fig. 1(b)).

The data, in figure 8, show that the configuration is statically stable throughout the angle-of-attack range investigated for each Mach number. These data also show that the static stability is insensitive to changes in Mach number from 4.5 to 9.0. Comparison of these data with the data at Mach number 13.5 shows that the combined influence of further increasing the Mach number and introducing ablation is very small. The insensitivity of the static stability to gas composition is also demonstrated. The stability decreases with increasing angle of attack which indicates that the variation of pitching moment with angle of attack is not linear for this configuration.

Estimates of C_{m_α} at zero angle of attack calculated by means of conical-flow theory (ref. 11) and Newtonian theory (ref. 12) are also included in this figure. Comparison of these theoretical estimates (valid only at zero angle of attack) with the experimental data shows both theories underestimate the initial stability by about 20 percent.

Several methods are available (refs. 13 to 17) which permit analysis of the observed pitching and yawing motions of a symmetrical body having a nonlinear pitching moment to obtain C_m as a function of α. The method of reference 17, developed under the assumption that the nonlinear moment can be described by an arbitrary integer-power series of the resultant angle of attack, was used to analyze the data obtained in the present tests. Application of this method to the data of this report is discussed in appendix A.

The local variations of pitching moment with angle of attack, extracted from the experimental data shown in figure 8 by the above procedure, are presented in figure 9. Examination of the experimental data at the three test Mach numbers shows, as expected, that the stability of the configuration is little affected by changes in Mach number from 4.5 to 13.5. The small increase in stability indicated at the higher angles of attack for an increase in Mach number from 4.5 to 9.0 could very well be considered within the accuracy of the experimental data at these angles of attack. The variation of pitching moment with angle of attack given by Newtonian theory and the initial slope calculated using conical-flow theory are also included in figure 9. As mentioned earlier, both theories underestimate the pitching moments at the low angles of attack by about 20 percent; however, Newtonian theory predicts an almost linear variation of C_m with α; whereas the experimental variation is seen to be slightly nonlinear with angle of attack. The agreement between experiment and theory, therefore, improves with increasing angle of attack and is considered close throughout the entire angle-of-attack range of this investigation.

Dynamic-Stability Characteristics

The results of the dynamic-stability measurements are presented in figure 10, where values of the dynamic-stability parameter, ξ, are plotted as a function of the maximum resultant angle of attack, σ_m. Negative values of ξ represent a convergent model motion (dynamic stability). These data show that the configuration is dynamically stable throughout the angle-of-attack range investigated for each Mach number and that it exhibits the same dynamic stability in air as it does in the carbon-dioxide--nitrogen mixture. These data also show that, within the scatter of the data, the values of ξ remain constant with increasing angle of attack and increasing Mach number. A value of ξ of -2.0 is a reasonable average for most of the data in figure 10, and is approximately equivalent to a convergence of about 7 percent per cycle. Examination of the data in figure 10 shows an appreciable amount of scatter in the values of ξ obtained at a Mach number of 13.5 for angles of attack below 10°. At these conditions, three flights gave values of ξ close to -7.0, which is approximately equivalent to a convergence of about 22 percent per cycle, and one flight gave a value of ξ of about +2.0, which is equivalent to a divergence of about 7 percent per cycle. To determine the largest reasonable variation in the experimental values of ξ for these flights, a probable error of 0.25° in angle-of-attack measurements, determined statistically from many readings by several observers, was introduced to the input data of these flights. These errors in the worst possible arrangements changed the values of ξ by less than ±1.0. Therefore, these values of ξ are considered representative of the actual damping characteristics experienced by the models in these flights.

There are several factors which might have contributed to the scatter of these data. One such factor is of the possibility of model damage. Calculations indicate that the stress at the bimetallic joint of the models could have, under an unusually high acceleration launch, equalled the compressive strength. The shadowgraphs from all the flights at Mach number 13.5 under high magnification, showed no evidence of deformation at the bimetallic joint but a very slight discontinuity in the bow-shock-wave angle of some of the models just ahead of the cylinder indicated there were surface deformations. Although a compressive failure of the titanium should not have caused this discontinuity since the stress here should have been less than that at the bimetallic joint, the sabots which grip this section of the models (see fig. 3(c)) could have caused small irregularities in the plastic coating. It was not possible, however, to correlate this effect with the values of ξ which produced the large scatter. Another possible explanation is that the scatter is due to effects of nonuniform ablation over the surface of some of the models and/or variations in the amount of ablation from flight to flight. Mass addition into the flow field about the body which resulted from ablation of the plastic is visible in the wakes in figures 5(c) and 6(c). It has been shown in reference 18 that mass addition could cause large changes in the static stability, and consequently in the dynamic stability, of a body moving at hypersonic speeds and that these changes in stability increase with increasing mass addition and depend on the angle of attack of the body. For the present tests, it was inferred from the experimental data presented in figures 7 and 8 that ablation effects were not sufficiently large to significantly affect the static stability and drag characteristics of the configuration; however, the dynamic stability might have been influenced. One other possibility is that the 1-1/2 cycles of oscillation at Mach number 13.5 (see fig. 4) constitute a minimal amount of motion for defining the dynamic-stability parameter when σ_m is small, especially when "trim" is present. Some or all of these possibilities could have contributed to the scatter in the dynamic-stability results at this Mach number.

Values of the damping-in-pitch derivative, $C_{m_q} + C_{m_{\dot{\alpha}}}$, were calculated by means of equation (5) using the values of ξ (fig. 10) and C_D (fig. 7) measured from the present tests, with values of C_{L_α} estimated by conical-flow theory, and are presented in figure 11 as a function of σ_m. These data show the same trends as those observed for the values of ξ in figure 10, namely, constant dynamic stability for the configuration throughout the Mach number and angle-of-attack range investigated. It is interesting to note that the values of $C_{m_q} + C_{m_{\dot{\alpha}}}$ have the same sign as the corresponding values of ξ and are about one-tenth as large. Thus, as seen from equation (5) the combination of a stabilizing lift-curve slope (positive value of C_{L_α}) and the stabilizing damping-in-pitch derivative overshadow the destabilizing contribution of drag to produce a convergent motion in constant speed flight at constant altitude.

Stability Characteristics for Large Amplitudes of Oscillation

The present configuration is intended to be statically stable about only one trim attitude, nose forward about zero angle of attack. Although experimental measurement of the amount of static instability (positive value of C_{m_α}) provided for in the design of the configuration about the base-forward trim attitude of 180° was beyond the scope of the present investigation, two exploratory flights were made with the models launched backward to determine whether they would remain flying backward or, as expected from calculations, would begin righting themselves to a nose-forward attitude. The models were launched at an initial angle of attack near 180° (see fig. 3(d)) at the same test conditions mentioned previously for the other flights at Mach number 9.0, namely, nominal model velocity of 3.05 km/sec and test-section static pressure of 4×10^4 newton/m^2 (300 mm of mercury).

The measured time history of the angular orientation for one of these flights (flight 703), presented in figure 12, shows that although there was only about one-half cycle of oscillation in the available 12.2-meter-length test section, the model did not remain in the base-forward orientation and did not tumble but achieved a nose-forward orientation and appeared to be oscillating about zero angle of attack with amplitudes of oscillation as large as 165°. This result indicates that the configuration is statically stable only about the nose-forward trim attitude of zero angle of attack. Another interesting and important possibility is suggested by this result and by the knowledge that for flight at constant or slightly decreasing dynamic pressure a model having negative or neutral dynamic stability would be expected to tumble. Since the model in this flight did not tumble, it is indicated that the dynamic-stability characteristics of the configuration, over this large-amplitude range, are such as to produce a convergent motion.

To investigate the dynamic-stability characteristics of the configuration over this large-amplitude range and to substantiate the result of flight 703 that the configuration has a unique nose-forward stable attitude, the second flight (flight 663) was conducted in the Ames Pressurized Ballistic Range (in air) which enabled the trajectory of the model to be recorded over a 62-meter length in 24 shadowgraph stations, thus providing several cycles of oscillation. The measured time history of the angular orientation for this flight presented in figure 13, along with that of flight 703, shows, as did flight 703, that the model did not remain in the base-forward orientation and did not tumble but again achieved a nose-forward orientation and oscillated about zero angle of attack with large amplitudes of oscillation. (It should be noted that the model experienced about a 68-percent decrease in dynamic pressure during this flight.) Further examination of the experimental data in this figure shows that although the time history for flight 663 is not as well defined as that for flight 703,[1] the model in this flight achieved almost exactly the same peak amplitude at the first peak of oscillation as did the

---

[1]Although the wave length of oscillation was approximately the same for both flights the observation stations in the PHFF facility are spaced at 1.22-meter intervals while the shortest spacing between the observation stations in the PBR is 2.13 meters.

model in flight 703. This almost exact duplication of the motions for both flights provides strong experimental evidence that the configuration is statically unstable about the trim angle of attack of 180° and will begin to overturn, immediately, to a nose-forward orientation and oscillate about its unique stable trim attitude of zero angle of attack. Since evaluation of the stability derivatives from analysis of the high-amplitude experimental data of flight 663 could not be accomplished using the method presented earlier (ref. 8) to extract these derivatives from low-amplitude motions, an attempt was made to generate a theoretical motion which would provide a good fit to the experimental data and allow the desired stability derivatives to be inferred. The differential equation of motion of a missile oscillating in pitch at constant altitude (see ref. 10), written with respect to time as

$$\ddot{\alpha} - \frac{qA}{mV} k_1 \dot{\alpha} - qAdC_m = 0 \tag{7}$$

where

$$k_1 = -C_{L_\alpha} + (C_{m_q} + C_{m_{\dot{\alpha}}})\left(\frac{d}{\sigma}\right)^2 \tag{8}$$

was programmed for numerical integration by a computer. Equation (7) was iterated upon to obtain the best match to the experimental data. The time variation of pitching moment with angle of attack given by Newtonian theory, the time variations of dynamic pressure and velocity measured for this flight, along with various values of k_1 were used as inputs for these calculations. These calculations were initiated at the first peak value of α, 164°, where the value of $\dot{\alpha}$ is zero. The theoretical motion obtained in this manner which best fit the experimental data is presented in figure 13 and is seen to be an excellent representation of the actual motion experienced by the model during this flight. This excellent agreement between the theoretical motion and the experimental data indicates that the pitching moments predicted by Newtonian theory for this configuration are very close to the actual pitching moments experienced by the model throughout the angle-of-attack range from 0° to 180°. (It should be noted that according to Newtonian theory the configuration is stable only in the nose-forward attitude.) Further examination of the data presented in figure 13 shows that the theoretical motion is convergent (the value of k_1 was -1.15 and, as can be seen, is equivalent to a convergence of about 4 percent per cycle), which indicates that the configuration is dynamically stable, about zero angle of attack, throughout the entire angle-of-attack range from 0° to 180°.

Application of the Present Results to a Full-Scale Vehicle Passively Entering the Atmosphere of Venus

To determine the significance of the present results when applied to a full-scale vehicle passively entering a planetary atmosphere, calculations were made of the oscillatory behavior of the present configuration, initially oriented base forward, flying an example entry trajectory through a model of the Venusian atmosphere. Studies of the oscillatory behavior of missiles entering the atmosphere on ballistic trajectories (ref. 19) have shown that the rapid increase in atmospheric density experienced by such vehicles strongly damps their oscillations. For the present example, two entry trajectories were considered: one, using an initial flight-path angle, γ_i of 89° which corresponds to a steep entry; and the other using a γ_i of 40°. These values for γ_i and the following assumed initial conditions were used to compute the entry trajectories for this example:

$$V_i = 11.43 \text{ km/sec}$$

$$y_i = 160 \text{ km}$$

$$m/C_D A = 156.8 \text{ kg/m}^2$$

The atmosphere used in these estimates was one selected on the basis of information presented in reference 20. As shown in reference 21, this atmosphere can be closely approximated by the well-known assumption that the atmospheric density varies exponentially with altitude

$$\rho = \rho_o e^{-\beta_V h}$$

for the altitudes between 160 km and 40 km (the altitudes of interest in the present example). This assumption and the following corresponding values of these parameters for Venus (see ref. 21) were applied to the present example:

$$\beta_V = 1.58\times10^{-4} \text{ per m}$$

$$\rho_o = 531 \text{ kg/m}^3$$

These conditions define the entry trajectories considered. Some of the trajectory parameters, namely, the variations of velocity and dynamic pressure with altitude, were computed using the above conditions in equations derived in reference 22 and are presented in figure 14. It can be seen from this figure that maximum dynamic pressure occurs at an altitude close to 65 km for both trajectories.

Analyses which describe the oscillatory motions developed by vehicles as they descend through a planetary atmosphere are presented in references 23 and 24. The analysis presented in reference 23 allows for an arbitrary initial angle of attack (nose forward or base forward) but assumes the aerodynamic damping of the vehicle to be zero. The analysis presented in reference 24 allows for aerodynamic damping of the vehicle but assumes constant aerodynamic coefficients which requires the vehicle to be initially oriented nose forward at a low angle of attack. Since the vehicle, for the present example, is to enter the Venusian atmosphere initially oriented base forward, the analysis of reference 23 was used to describe the oscillatory motions for the portion of the trajectory for which the aerodynamic damping of the vehicle could, in fact, be considered negligible compared to damping due to increasing dynamic pressure (see ref. 19). This analysis showed the vehicle to be oriented nose forward and oscillating at low angles of attack at a point in the trajectory prior to reaching q_{max}. It was therefore possible to use reference 24 to determine the effect of the measured damping on vehicle motions for the remainder of the trajectory.

Reference 23 shows that under the assumptions made in the analysis the envelope of these oscillations, expressed in terms of significant vehicle and planetary properties, can be written as

$$\frac{(\tan \epsilon)env}{\tan \epsilon_p} = CG\left[\frac{-\beta_V{}^2 \sin^2 \gamma_i I_y}{2\rho_o AdC_{m_{max}}} e^{\beta_V h} e^{(C_D\rho_o A/\beta_V m \sin \gamma_i)e^{-\beta_V h}}\right]^{1/4} \tag{9}$$

For the present examples, the vehicle was assumed to be initially oriented base forward at an angle of attack of 179°, with zero initial pitch rate, which gives values of the parameters C and G of 0.796 and 0.0215, respectively. (The parameters C and G are dependent on the initial angle of attack and initial pitch rate assumed and cannot be evaluated explicitly; their values are determined from charts presented in reference 23.) The following physical properties of the vehicle were assumed

$$A = 0.771 \text{ m}^2$$

$$d = 1.0 \text{ m}$$

$$I_y = 6.44 \text{ kg-m}^2$$

$$m = 6.66 \text{ kg}$$

$$C_D = 0.55$$

$$C_{m_{max}} = -0.0835$$

where $C_{m_{max}}$ is the maximum value of pitching moment estimated using Newtonian theory. Values of the envelopes of oscillations, $(\alpha)_{env}$, computed are presented in figure 15 as a function of altitude. The results in this figure show that for that portion of the entry prior to q_{max} the motions, for both entries, converge very rapidly so that at the altitudes where heating is most severe (between 80 km and 65 km, see fig. 14), the amplitudes of oscillation of the vehicle are less than 35°. These results also show that for the altitudes subsequent to q_{max}, an analysis which assumes the aerodynamic damping of the vehicle is zero predicts highly divergent motions. However, as was shown in figure 10, the present configuration possesses positive aerodynamic damping and the effect of this positive damping on the oscillatory motions must be included in the analysis.

Reference 24 shows that for constant aerodynamic derivatives the envelope of oscillations has the simple form

$$\alpha_{max} = \frac{C_1 u^{-K/2}}{q_\infty{}^{1/4}} \tag{10}$$

It also has been shown in this reference that the dynamic-stability parameter K, in the form

$$K = \frac{1}{C_D}\left[-C_{L_\alpha} + (C_{m_q} + C_{m_{\dot{\alpha}}})\left(\frac{d}{\sigma}\right)^2\right] \tag{11}$$

is a convenient parameter for describing the dynamic stability of a vehicle descending through a planetary atmosphere. It can be seen from a comparison of equations (5) and (11) that K can be expressed in terms of ξ and C_D as follows

$$K = \frac{\xi}{C_D} - 1 \tag{12}$$

Values of K computed from the measured values of ξ (fig. 10) and C_D (fig. 7) are presented in figure 16 as a function of σ_m. From these data it was considered that a value of K of -3.0 would be a conservative mean value to use in equation (10). This value of K and the example entry trajectories presented earlier were introduced into equation (10), expressed in ratio form, and values of the amplitude ratio, $(\alpha/\alpha_i)_{max}$, were computed. These calculations were initiated at an altitude of 80 km, since, as can be seen from figure 15, the oscillatory angles of attack of the vehicle below this altitude are less than 36° and, as demonstrated in figures 9 and 16, the aerodynamic derivatives of the configuration can be considered reasonably constant in this angle-of-attack range. Values of $(\alpha)_{env}$ were computed from the ratio $(\alpha/\alpha_i)_{max}$ using the angles of attack at 80 km given by the analysis of reference 23 as initial angles of attack (36° for the $\gamma_i = 89°$ case and 30° for the $\gamma_i = 40°$ case) and are presented in figure 15. These results show that at altitudes below that for q_{max} the effect of the measured aerodynamic damping of the configuration overshadows the effect of decreasing dynamic pressure to produce a strongly convergent motion. The amplitudes of oscillation at an altitude of 56 km for both examples are seen to be less than 5°. Therefore, from these calculations it is indicated that the present configuration, initially oriented nose forward or base forward, should experience highly convergent pitching oscillations during entry into the postulated atmosphere of Venus.

SUMMARY OF RESULTS

The results of an experimental investigation to determine the stability and drag characteristics of a conical configuration at Mach numbers of 4.5, 9.0, and 13.5 and Reynolds numbers from 0.4 to 1.2 million in a N_2-CO_2 mixture and in air are as follows:

1. The static stability, dynamic stability, and drag of the configuration are the same in air as in a gas mixture composed of 9-percent carbon dioxide and 91-percent nitrogen for the entire range of Mach numbers and angles of attack of this investigation.

2. The configuration is statically stable about an angle of attack of 0° (nose-forward orientation) for the assumed location of center of gravity, 0.72 d from the nose. Strong evidence is presented which shows that the configuration is statically unstable about a trim angle of attack of 180° (base-forward orientation), so that, if initially oriented base forward, it will reorient itself to a nose-forward attitude. The static stability is essentially invariant with Mach number and slightly nonlinear with angle of attack in the angle range up to 40°.

3. The nonlinear variation of pitching moment with angle of attack was closely approximated by a two-term power series of the resultant angle of attack.

4. The configuration is dynamically stable for steady flight at constant altitude. For this condition and for initial amplitudes of oscillation as high as 40°, the models experienced pitching motions which converged at the rate of about 7 percent per cycle. Also, there is strong indication that the configuration is dynamically stable at pitching amplitudes approaching 180° so that it will oscillate about the nose-forward stable attitude with diminishing amplitude of oscillation. Analysis of the large amplitude oscillations of a model concurrently experiencing a rapid decrease in dynamic pressure with time showed a convergence of about 4 percent per cycle.

5. The drag coefficient of the configuration decreases approximately 8 percent for an increase in Mach number from 4.5 to 9.0 but remains constant for a further increase in Mach number to 13.5. The drag increases approximately 30 percent, for each Mach number, as the angle of attack is increased from 0° to about 28°.

6. The variation of pitching moment with angle of attack given by Newtonian theory is in close agreement with the measured variation for the angle-of-attack range from 0° to about 36°, although Newtonian theory and conical-flow theory underestimate the initial slope by about 20 percent. Furthermore, it is indicated that Newtonian theory gives close estimates of the pitching moments of this configuration for the entire angle-of-attack range from 0° to 180°. The drag of the configuration was accurately estimated by conical-flow theory at zero angle of attack and was closely approximated by Newtonian theory for the angle-of-attack range investigated, 0° to about 28°.

7. Calculations indicate that the measured stability characteristics of the present configuration should be adequate for orienting the vehicle properly during a Venus entry. For any initial orientation of the vehicle (nose forward or base forward) the pitching motions should converge to a very small fraction of the amplitude at entry.

Ames Research Center
National Aeronautics and Space Administration
Moffett Field, Calif., Dec. 18, 1964

APPENDIX A

APPLICATION OF NONLINEAR PITCHING-MOMENT ANALYSIS

A method which permits analysis of the pitching and yawing motions of a spinning symmetrical body having a nonlinear pitching moment to obtain the pitching moment as a function of angle of attack is described in reference 17. The method allows for a more general reduction of free-flight data by assuming that the restoring moment can be described by an arbitrary power series of the resultant angle of attack, of the form

$$M(\sigma) = -\sum_{n=0}^{\infty} M_n \sigma^{n+1} \tag{A1}$$

where

$$M(\sigma) = \frac{qAd}{I} C_m \tag{A2}$$

A simple expression is then derived which relates the frequency of oscillation, ω, obtained from data analysis with linear equations, to the maximum and minimum amplitudes for an infinite number of possible moment combinations. This expression, which includes the nonlinear inertial terms due to spin, is (see ref. 17)

$$\omega^2 = \frac{8 \displaystyle\sum_{n=0}^{\infty} \frac{M_n}{n+2} \left[\frac{\sigma_m^{n+4} + \sigma_o^{n+4}}{2} - \left(\frac{\sigma_m^2 + \sigma_o^2}{2} \right)^{\frac{n+4}{2}} \right]}{(\sigma_m^2 + \sigma_o^2)^2} \tag{A3}$$

By use of this expression, values of the restoring-moment coefficients, M_n, can be obtained from the observed frequencies of oscillation and amplitudes of independent flights of the models at similar flight conditions but with different amplitudes of oscillation. Equation (A3), as discussed in reference 17, is an approximate solution which becomes exact in the limit of circular motion, that is, equal pitch and yaw, 90° out of phase and is least accurate for the case of planar motion. As can be seen from examination of figure 4, the motions to be analyzed for the present investigation are fairly planar. However, the applicability of the method to the case of planar motion was examined in reference 17 for certain assumed moment representations for which exact solutions are possible. Comparison showed that the approximate solution (eq. (A3)) gives results extremely close to the results obtained from exact solutions. Further comparison in reference 17 shows, again for the case of planar motion, that the approximate solution gives results that are, for the most part, more accurate than results obtained by the technique of reference 13. Therefore, a high degree of confidence in the applicability of this method to the data of this report is justified.

Application of the method to the present experimental data was accomplished in the following manner. Equation (A3), which allows for an infinite number of possible moment combinations, was limited, from practical considerations, to the first seven terms written as

$$
\begin{aligned}
\frac{qAd}{I} C_{m_\alpha} = M_o + \frac{8}{3} M_1 \frac{\dfrac{\sigma_m^{\ 5} + \sigma_o^{\ 5}}{2} - \left(\dfrac{\sigma_m^{\ 2} + \sigma_o^{\ 2}}{2}\right)^{\frac{5}{2}}}{(\sigma_m^{\ 2} - \sigma_o^{\ 2})^2} \\
+ \frac{3}{4} M_2(\sigma_m^{\ 2} + \sigma_o^{\ 2}) + \frac{8}{5} M_3 \frac{\dfrac{\sigma_m^{\ 7} + \sigma_o^{\ 7}}{2} - \left(\dfrac{\sigma_m^{\ 2} + \sigma_o^{\ 2}}{2}\right)^{\frac{7}{2}}}{(\sigma_m^{\ 2} - \sigma_o^{\ 2})^2} \\
+ \frac{1}{12} M_4(7\sigma_m^{\ 4} + 10\sigma_m^{\ 2} + 7\sigma_o^{\ 4}) + \frac{8}{7} M_5 \frac{\dfrac{\sigma_m^{\ 9} + \sigma_o^{\ 9}}{2} - \left(\dfrac{\sigma_m^{\ 2} + \sigma_o^{\ 2}}{2}\right)^{\frac{9}{2}}}{(\sigma_m^{\ 2} + \sigma_o^{\ 2})^2} \\
+ \frac{5}{32} M_6(3\sigma_m^{\ 6} + 5\sigma_m^{\ 4}\sigma_o^{\ 2} + 5\sigma_m^{\ 2}\sigma_o^{\ 4} + 3\sigma_o^{\ 6})
\end{aligned}
\tag{A4}
$$

(For convenience, since values of C_{m_α} are available from the linear analysis of the experimental data, the substitution $\omega^2 = (qAd/I_y)C_{m_\alpha}$ was made in equation (A4).) An examination of the experimental data in figure 8 indicated that the nonlinearities could not be considered large; therefore, it was decided that a two- or three-term moment in the resultant angle of attack would adequately represent the moment curve. Equation (A4) was programmed for machine computation so that all possible moment combinations, each containing the linear term, M_o, plus one and two members of the set (M_1, M_2, M_3, M_4, M_5, M_6) were fitted to the data by the method of least squares. The results are presented in figure 17, which shows the pitching-moment curves given by the various assumed moment representations that best fit the experimental data for each Mach number. The linear plus cubic pitching-moment curves are also included in this figure. (These pitching-moment curves are the same as would be obtained by the method of reference 15, which develops this case exclusively.) It is evident from these results that for the angle-of-attack range investigated the moment curves given by the best two- and three-term moment approximations for a particular Mach number are close enough together that it is unnecessary to choose between them. Furthermore, since the results show that the nonlinear pitching moment can be closely approximated by the simplest of the moment representations tried, namely, a two-term moment representation, the applicability of the method to the data of this report rests on the approximate linear relationship of C_{m_α} with the maximum and minimum amplitudes of the motion. Therefore, in order to determine the validity of this assumption, values of C_{m_α} were plotted as a function of the appropriate amplitude term given in equation (A4) for a one-three moment representation at

Mach number 4.5 and for a one-four moment representation at Mach numbers 9.0 and 13.5 for each flight and are presented in figure 18. It is evident from this figure that the data fall very closely along straight lines for each Mach number and, therefore, the particular two-term moment representations of the method are excellent approximations.

REFERENCES

1. Allen, H. Julian; Seiff, Alvin; and Winovich, Warren: Aerodynamic Heating of Conical Entry Vehicles at Speeds in Excess of Earth Parabolic Speed. NASA TR R-185, 1963.

2. James, Carlton S.; and Smith, Willard G.: Experimental Studies of Static Stability and Radiative Heating Associated With Mars and Venus Entry. Proc. Aerospace Forum, 1st Session, N. Y., IAS, SMF Fund Paper FF-34, 1963, pp. 16-21.

3. Demele, Fred A.: A Study of the Convective and Radiative Heating of Shapes Entering the Atmospheres of Venus and Mars at Superorbital Speeds. NASA TN D-2064, 1963.

4. Kellogg, William W.; and Sagan, Carl: The Atmospheres of Mars and Venus. Pub. 944, Natl. Acad. of Sci., National Research Council, 1961.

5. Curtis, John S.: An Accelerated Reservoir Light-Gas Gun. NASA TN D-1144, 1962.

6. Seiff, Alvin: A New Method for Computing Drag Coefficients From Ballistic Range Data. J. Aero. Sci., vol. 25, no. 2, Feb. 1958, pp. 133-134.

7. Seiff, Alvin; and Wilkins, Max E.: Experimental Investigation of a Hypersonic Glider Configuration at a Mach Number of 6 and at Full-Scale Reynolds Numbers. NASA TN D-341, 1961.

8. Nicolaides, John D.: On the Free Flight Motion of Missiles Having Slight Configurational Asymmetries. BRL Rep. 858, Aberdeen Proving Ground, Md., 1953.

9. Short, Barbara J.; and Sommer, Simon C.: Some Measurements of the Dynamic and Static Stability of Two Blunt-Nosed, Low-Fineness-Ratio Bodies of Revolution in Free Flight at $M = 4$. NASA TM X-20, 1959.

10. Seiff, Alvin; Sommer, Simon C.; and Canning, Thomas N.: Some Experiments at High Supersonic Speeds on the Aerodynamic and Boundary-Layer Transition Characteristics of High-Drag Bodies of Revolution. NACA RM A56I05, 1957.

11. Staff of the Computing Section, M.I.T., under the direction of Zdenek Kopal: Tables of Supersonic Flow Around Yawing Cones. Tech. Rep. 3, Cambridge, 1947.

12. Margolis, Kenneth: Theoretical Evaluation of the Pressures, Forces, and Moments at Hypersonic Speeds Acting on Arbitrary Bodies of Revolution Undergoing Separate and Combined Angle-of-Attack and Pitching Motions, NASA TN D-652, 1961.

13. Kryloff, N.; and Bogoliuboff, N. (Solomon Lefschetz, trans.): Introduction to Non-Linear Mechanics. Annals of Mathematics Studies, no. 11, Princeton Univ. Press, 1943.

14. Murphy, Charles H.: The Measurement of Non-Linear Forces and Moments by Means of Free-Flight Tests. BRL Rep. 974, Aberdeen Proving Ground, 1956.

15. Rasmussen, Maurice L.: Determination of Nonlinear Pitching-Moment Characteristics of Axially Symmetric Models From Free-Flight Data. NASA TN D-144, 1960.

16. Kirk, Donn B.: A Method for Obtaining the Nonlinear Aerodynamic Stability Characteristics of Bodies of Revolution From Free-Flight Tests. NASA TN D-780, 1961.

17. Rasmussen, Maurice L.; and Kirk, Donn B.: On the Pitching and Yawing Motion of a Spinning Symmetric Missile Governed by an Arbitrary Nonlinear Restoring Moment. NASA TN D-2135, 1964.

18. Syvertson, Clarence A.; and McDevitt, John B.: Effects of Mass Addition on the Stability of Slender Cones at Hypersonic Speeds. AIAA Jour., vol. 1, no. 4, April 1963, pp. 939-940.

19. Friedrich, Hans R.; and Dore, Frank J.: The Dynamic Motion of a Missile Descending Through the Atmosphere. J. Aero. Sci., vol. 22, no. 9, Sept. 1955, pp. 628-632, 638.

20. Kaplan, Lewis D.: A Preliminary Model of the Venus Atmosphere. Tech. Rep. 32-379, JPL, Dec. 1962.

21. Seiff, Alvin: Some Possibilities for Determining the Characteristics of the Atmospheres of Mars and Venus From Gas-Dynamic Behavior of a Probe Vehicle. NASA TN D-1770, 1963.

22. Allen, H. Julian; and Eggers, A. J., Jr.: A Study of the Motion and Aerodynamic Heating of Ballistic Missiles Entering the Earth's Atmosphere at High Supersonic Speeds. NACA Rep. 1381, 1958.

23. Tobak, Murray; and Peterson, Victor L.: Theory of Tumbling Bodies Entering Planetary Atmospheres With Application to Probe Vehicles and the Australian Tektites. NASA TR R-203, July 1964.

24. Sommer, Simon C.; and Tobak, Murray: Study of the Oscillatory Motion of Manned Vehicles Entering the Earth's Atmosphere. NASA MEMO 3-2-59A, 1959.

TABLE I.- TEST CONDITIONS, MODEL MEASUREMENTS, AND TEST RESULTS

Flight	Test gas	M	Re×10^{-6}, based on d	C_D	C_{m_α} (linear), $\frac{x_{cg}}{d}$ = 0.72	ξ	$C_{m_q} + C_{m_{\dot\alpha}}$	K	σ_m, deg	σ_o, deg	σ_{rms}, deg	d, cm	$\frac{x_{cg}}{d}$	Mass, g	I_y×10^8, kg-m^2	$\left(\frac{d}{\sigma}\right)^2$
(a) Nominal Mach number = 4.5																
707	9% CO_2-91% N_2	4.27	0.380	0.631	-0.101	-1.65	-0.16	-3.61	8.25	0.58	5.61	1.015	0.719	1.732	2.11	8.48
708		4.46	.390	.614	-.098	-1.33	-.12	-3.17	6.39	.33	4.62	1.013	.716	1.734	2.08	8.57
709		4.55	.398	.612	-.098	-3.44	-.36	-6.62	5.04	.31	3.26	1.012	.718	1.728	2.08	8.50
710		4.56	.398	.613	-.100	-1.91	-.18	-4.12	5.75	.24	3.88	1.014	.718	1.738	2.11	8.48
813		4.50	.370	.681	-.097	-1.46	-.14	-3.14	19.68	.97	13.15	1.013	.716	1.752	2.15	8.36
815		4.35	.395	.650	-.097	-1.52	-.14	-3.34	15.39	2.54	10.29	1.014	.718	1.745	2.10	8.53
816		4.50	.404	.631	-.101	-3.10	-.33	-5.91	10.95	2.21	7.52	1.016	.724	1.740	2.12	8.46
817		4.49	.402	.625	-.105	-1.91	-.19	-4.06	9.74	.58	6.59	1.016	.720	1.752	2.14	8.44
818		4.50	.397	.626	-.103	-2.45	-.25	-4.91	7.48	.33	4.89	1.010	.723	1.728	2.07	8.50
820		4.23	.375	.633	-.103	-1.24	-.11	-2.96	8.43	.61	5.84	1.014	.720	1.734	2.09	8.55
846		4.47	.412	.616	-.103	-0.86	-.06	-2.40	7.32	.14	4.95	1.018	.717	1.755	2.12	8.61
847		4.32	.390	.637	-.102	-1.12	-.09	-2.75	9.27	.33	6.20	1.018	.720	1.733	2.09	8.59
848		4.49	.412	.610	-.102	-2.08	-.20	-4.41	5.02	.20	3.14	1.015	.722	1.750	2.09	8.63
947		4.40	.399	.804	-.073	-1.23	-.13	-2.53	39.34	.29	27.19	1.015	.721	1.734	2.12	8.46
948		4.71	.435	.672	-.095	-2.13	-.22	-4.17	22.07	1.89	14.40	1.016	.723	1.728	2.11	8.45
950		4.32	.379	.742	-.088	-2.18	-.23	-3.94	30.32	1.27	20.94	1.016	.723	1.725	2.11	8.47
951		4.64	.431	.774	-.079	-1.69	-.18	-3.18	35.27	1.43	25.23	1.016	.716	1.734	2.12	8.46
958		4.64	.424	.733	-.089	-1.45	-.15	-2.98	29.10	1.09	19.89	1.014	.716	1.753	2.13	8.46
962		4.70	.434	.611	-.105	-1.87	-.18	-4.06	7.70	.43	5.33	1.015	.719	1.730	2.12	8.41
1173		4.58	.412	.822	-.076	-0.84	-.08	-2.02	38.27	2.04	27.73	1.015	.717	1.785	2.14	8.62
1183		4.52	.411	.823	-.074	-1.49	-.16	-2.81	41.29	6.31	29.07	1.014	.722	1.738	2.09	8.54
711	Air	4.51	.408	.605	-.100	-2.68	-.28	-5.43	5.59	.34	3.83	1.014	.720	1.739	2.14	8.23
853		4.02	.421	.702	-.090	-1.05	-.09	-2.50	23.48	.98	16.15	1.052	.732	1.830	2.32	8.73
963		4.59	.416	.830	-.071	-2.35	-.26	-3.83	40.64	1.21	28.12	1.015	.722	1.734	2.13	8.40
(b) Nominal Mach number = 9.0																
698	9% CO_2-91% N_2	9.03	.810	.561	-.103	-0.89	-.06	-2.59	8.07	.36	5.70	1.014	.718	1.735	2.10	8.09
699		8.89	.766	.581	-.096	-1.76	-.17	-4.03	11.93	.57	8.35	1.013	.719	1.731	2.10	8.00
700		9.40	.841	.586	-.093	-1.68	-.16	-3.87	13.84	.60	9.91	1.014	.721	1.728	2.10	8.14
701		8.90	.794	.567	-.097	-2.54	-.26	-5.48	9.56	.49	6.44	1.014	.718	1.738	2.10	8.14
702		8.93	.813	.561	-.095	-2.56	-.27	-5.56	7.96	.42	5.44	1.014	.720	1.744	2.11	8.12
805		9.16	.825	.611	-.091	---	---	---	19.45	4.37	14.66	1.015	.723	1.685	2.04	8.52
806		8.81	.778	.569	-.093	-1.80	-.16	-4.16	4.43	.23	3.11	1.015	.716	1.715	2.12	8.35
807		8.94	.812	.595	-.096	-1.62	-.15	-3.72	14.67	1.99	9.87	1.014	.716	1.707	2.09	8.40
808		8.63	.773	.620	-.096	-2.08	-.21	-4.35	20.38	.77	14.08	1.018	.722	1.733	2.13	8.44
809		8.38	.759	.710	-.088	-1.60	-.16	-3.25	31.15	2.28	21.85	1.020	.722	1.735	2.12	8.52
810		9.91	.885	.637	-.092	-2.44	-.25	-4.83	22.62	3.39	15.76	1.018	.716	1.750	2.14	8.47
952		9.13	.758	.598	-.100	-1.58	-.14	-3.64	16.20	.81	10.61	1.016	.723	1.735	2.12	8.47
953		9.23	.852	.610	-.101	-2.32	-.23	-4.80	19.13	1.24	12.56	1.016	.721	1.749	2.12	8.51
954		9.71	.888	.616	-.093	-1.88	-.18	-4.05	20.53	.10	13.66	1.016	.723	1.720	2.11	8.40
955		9.44	.967	.609	-.094	-1.32	-.12	-3.17	19.71	1.25	13.22	1.015	.720	1.725	2.13	8.36
956		9.19	.850	.610	-.097	-1.82	-.17	-3.98	18.72	.90	12.43	1.014	.721	1.735	2.12	8.41

TABLE I.- TEST CONDITIONS, MODEL MEASUREMENTS, AND TEST RESULTS - Concluded

Flight	Test gas	M	$Re \times 10^{-6}$, based on d	C_D	C_{m_α} (linear), $\frac{x_{cg}}{d} = 0.72$	ξ	$C_{m_q} + C_{m_{\dot{\alpha}}}$	K	σ_m, deg	σ_o, deg	σ_{rms}, deg	d, cm	$\frac{x_{cg}}{d}$	Mass, g	$I_y \times 10^8$, kg-m^2	$\left(\frac{d}{\sigma}\right)^2$
(b) Nominal Mach number = 9.0 - Concluded																
957	9% CO_2-91% N_2	9.28	0.871	0.631	-0.096	-1.71	-0.16	-3.71	23.18	1.24	14.83	1.015	.719	1.742	2.12	8.45
959		9.30	.847	.600	-.099	-1.79	-.17	-3.98	17.87	1.92	11.79	1.015	.719	1.748	2.15	8.37
960		9.46	.871	.578	-.093	-1.15	-.26	-2.99	13.05	2.04	8.76	1.015	.718	1.738	2.14	8.38
1171		9.17	.835	.613	-.099	-2.70	-.28	-5.40	18.66	4.19	12.47	1.015	.718	1.733	2.12	8.45
1174		8.63	.796	.594	-.100	-3.27	-.35	-6.50	15.27	3.92	10.49	1.015	.717	1.742	2.14	8.40
1182		8.95	.825	.736	-.086	-1.74	-.18	-3.36	35.77	3.53	25.05	1.013	.718	1.752	2.11	8.54
1184		8.92	.791	.609	-.102	-1.77	-.17	-3.91	17.97	2.30	12.23	1.013	.717	1.740	2.11	8.50
697	Air	8.97	.827	.555	-.096	-2.81	-.30	-6.06	7.56	.21	5.06	1.013	.719	1.730	2.10	8.02
804		8.16	.727	.558	-.101	-2.43	-.24	-5.06	7.78	.52	5.11	1.014	.718	1.749	2.15	8.36
965		9.33	.841	.582	-.097	-2.36	-.24	-5.05	15.17	3.39	10.12	1.016	.720	1.732	2.13	8.40
1170		8.84	.815	.617	-.094	-2.42	-.25	-4.92	21.00	4.17	14.05	1.015	.719	1.740	2.14	8.40
703	9% CO_2-91% N_2	8.36	.721	---	---	---	---	---	164	0	---	1.015	.720	1.736	2.11	8.45
663	Air	6.94	.604	.879	---	---	---	---	164	0	---	1.015	.720	1.730	2.10	8.47
(c) Nominal Mach number = 13.5																
978	9% CO_2-91% N_2	14.32	1.25	.552	-.095	-.77	-.04	-2.40	1.98	.79	1.32	1.052	.728	2.865	3.43	9.22
979		14.01	1.28	.603	-.096	-3.06	-.29	-6.07	19.65	2.67	13.98	1.053	.735	2.869	3.43	9.282
982		13.44	1.30	.560	-.105	+2.21	+.28	+2.95	8.34	1.26	5.87	1.051	.734	2.848	3.38	9.31
983		13.56	1.31	.551	-.100	-1.57	-.12	-3.85	8.52	1.29	5.93	1.054	.738	2.861	3.41	9.34
985		13.31	1.24	.710	-.091	-3.52	-.35	-5.96	29.15	1.83	21.38	1.052	.728	2.856	3.42	9.25
986		13.64	1.32	.558	-.100	-6.56	-.66	-12.76	8.56	.40	6.38	1.054	.732	2.861	3.39	9.36
988		13.43	1.27	.553	-.099	-4.27	-.41	-8.72	4.04	.32	2.76	1.054	.727	2.862	3.41	9.33
989		13.75	1.29	.563	-.099	-3.17	-.30	-6.63	11.95	1.64	8.22	1.054	.730	2.856	3.41	9.31
1178		13.72	1.27	.565	-.102	-5.07	-.51	-9.97	9.91	2.46	7.19	1.054	.733	2.858	3.46	9.18
1181		13.82	1.29	.585	-.095	-2.22	-.20	-4.80	16.94	1.51	11.93	1.054	.731	2.850	3.44	9.21
987	Air	13.89	1.30	.545	-.095	-2.65	-.24	-5.86	3.77	.76	2.75	1.054	.736	2.857	3.37	9.42
1169		13.85	1.34	.552	-.099	-1.93	-.16	-4.50	7.06	.94	5.06	1.054	.733	2.858	3.39	9.37
1177		13.77	1.28	.547	-.098	-7.68	-.79	-15.03	5.57	1.28	4.01	1.053	.731	2.872	3.47	9.18
1180		13.74	1.27	.534	-.100	-7.11	-.72	-14.30	1.41	.36	1.01	1.054	.738	2.862	3.45	9.23

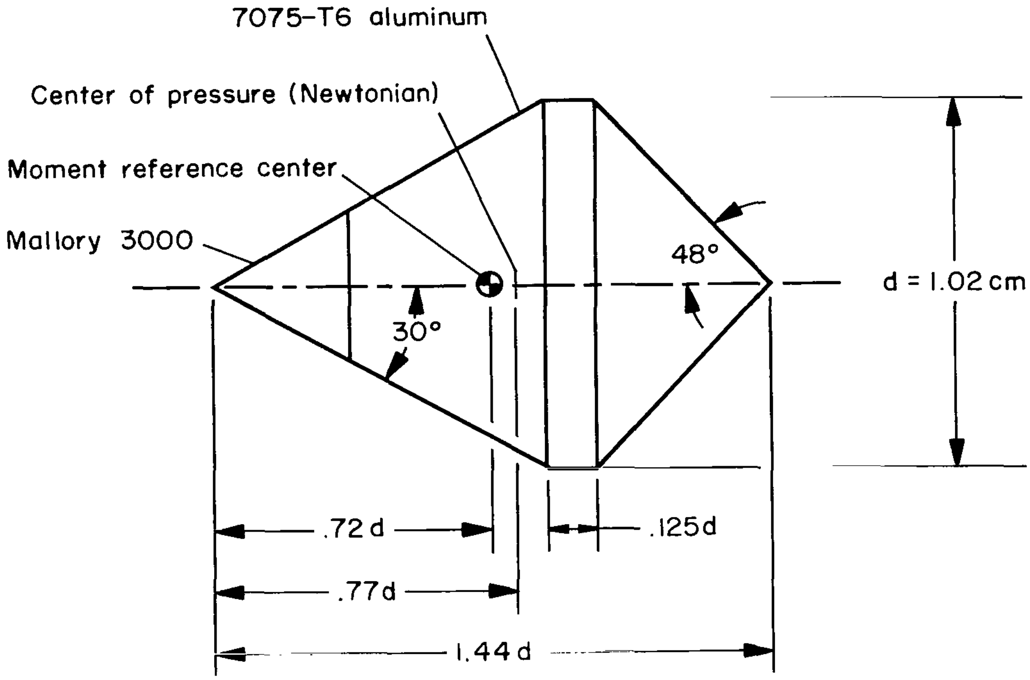

(a) Model.

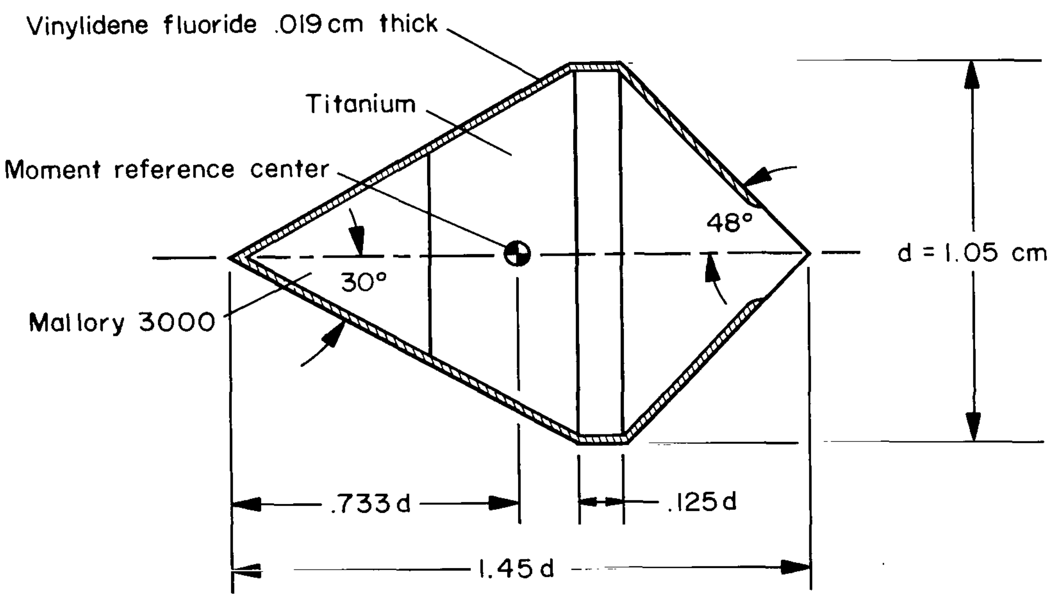

(b) Plastic-coated model.

Figure 1.- Sketches of models showing nominal dimensions.

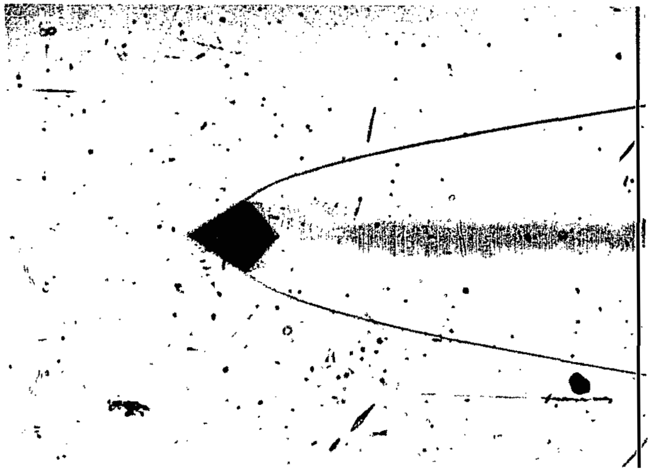

First station.

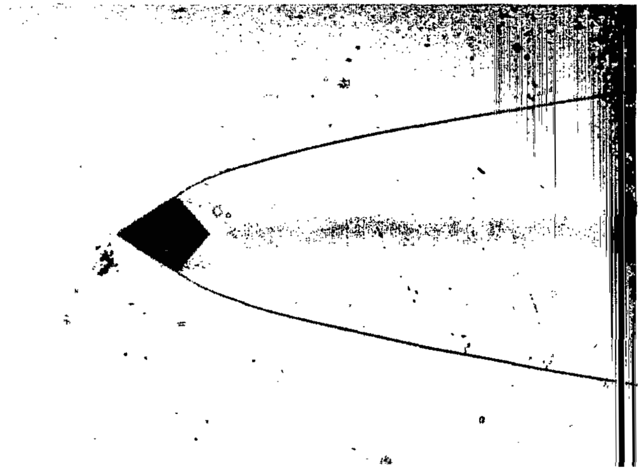

Last station.

(a) N_2-CO_2

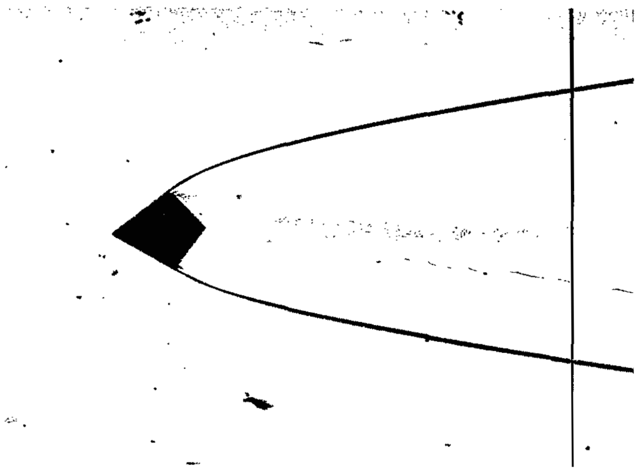

First station.

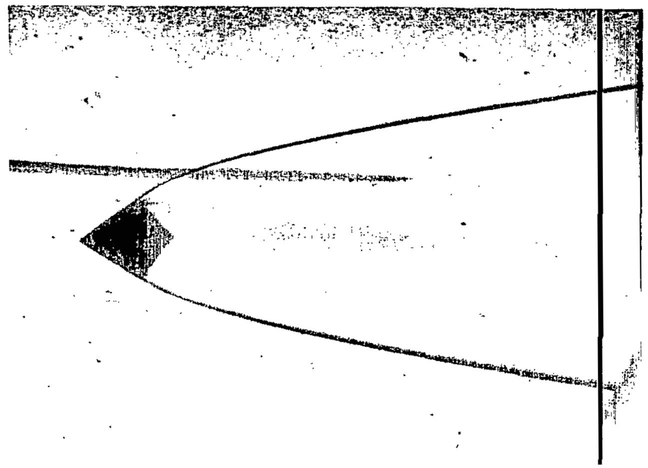

Last station.

(b) Air

Figure 2.- Shadowgraphs showing negligible tip blunting on ablating plastic-coated models; $M = 13.5$.

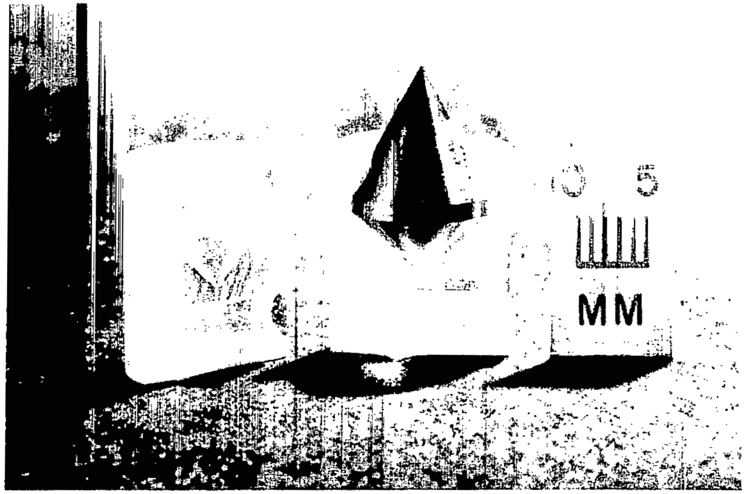

(a) Model with straight sabot.

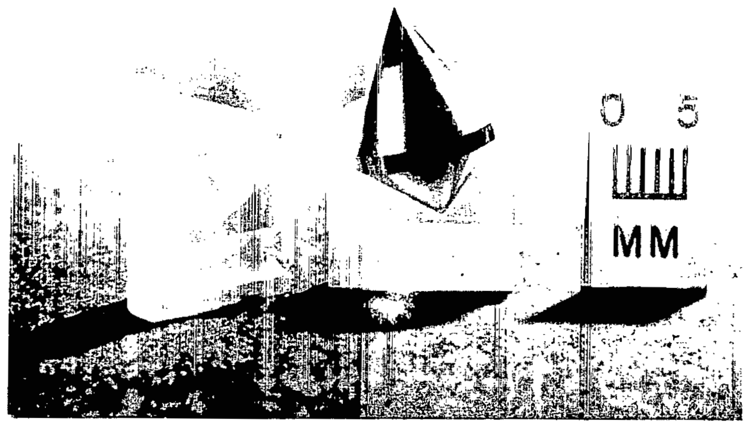

(b) Model with canted sabot.

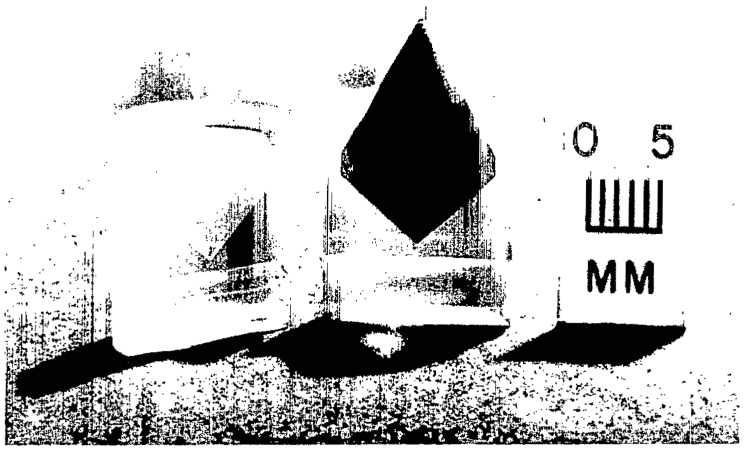

(c) Plastic-coated model with straight sabot.

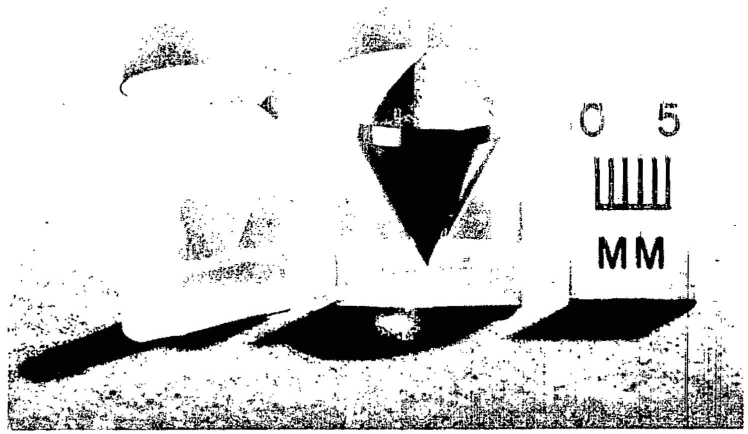

(d) Model with sabot for base-forward launch.

Figure 3.- Photographs of models and sabots.

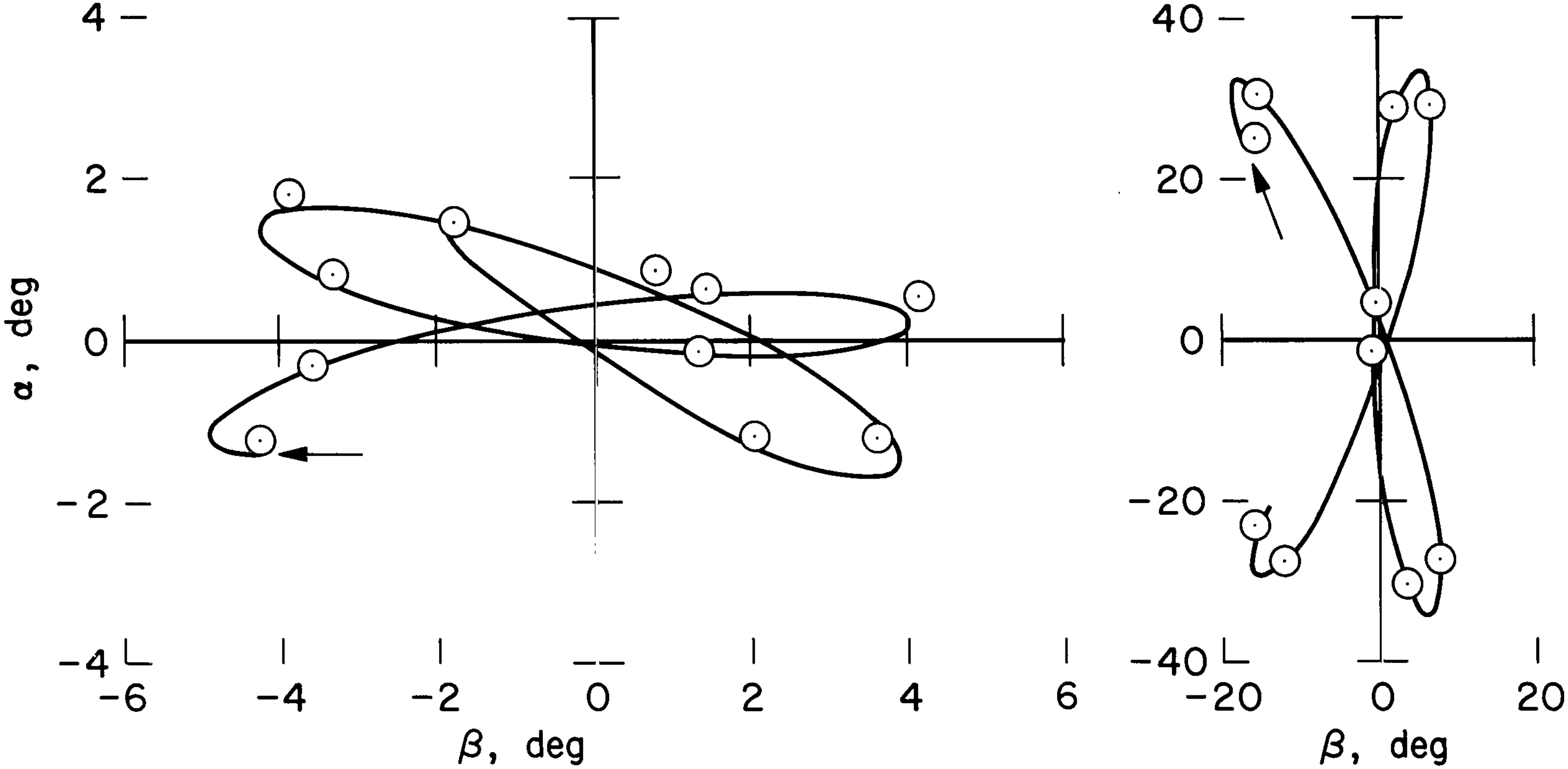

(a) Flight 848; M = 4.5

(b) Flight 951; M = 4.5

Figure 4.- Typical pitching and yawing motions produced by the models.

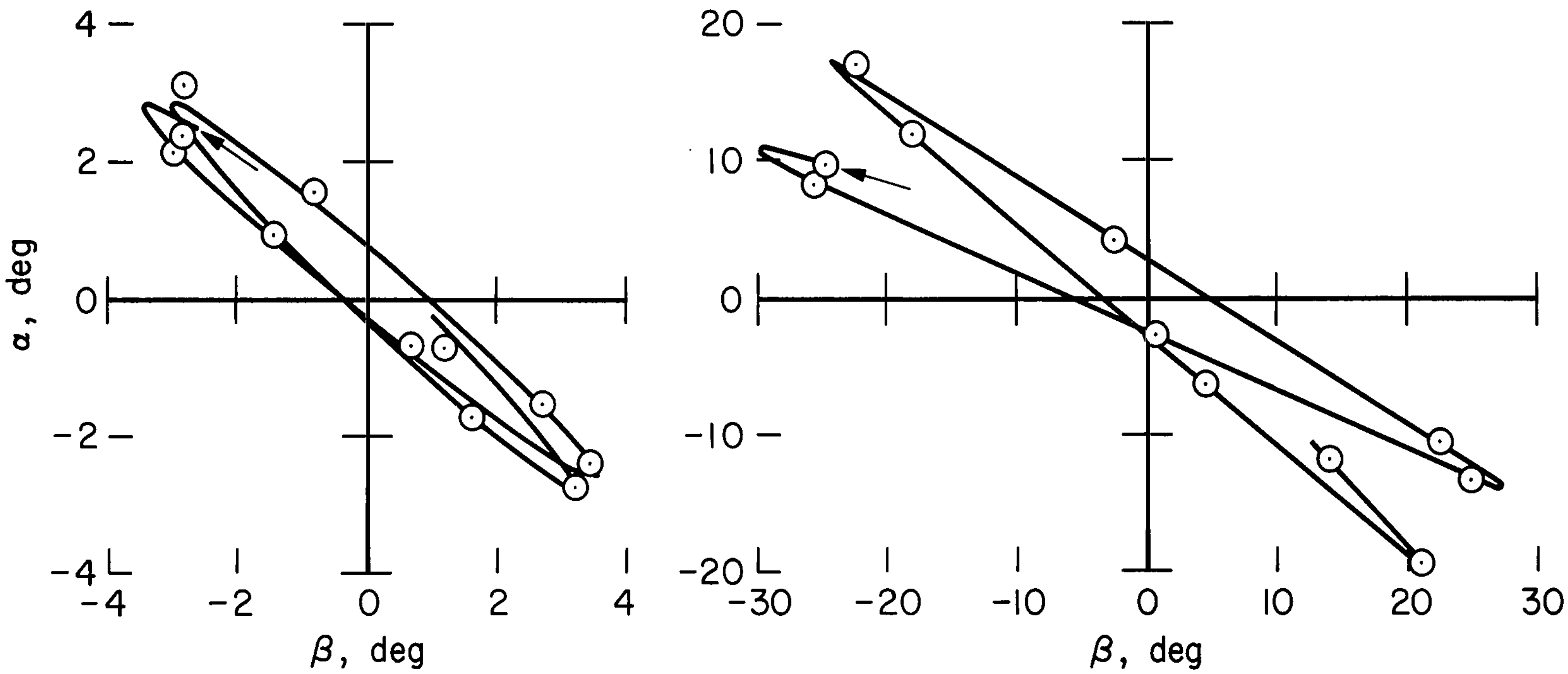

(c) Flight 806; M = 9.0

(d) Flight 809; M = 9.0

Figure 4.- Continued.

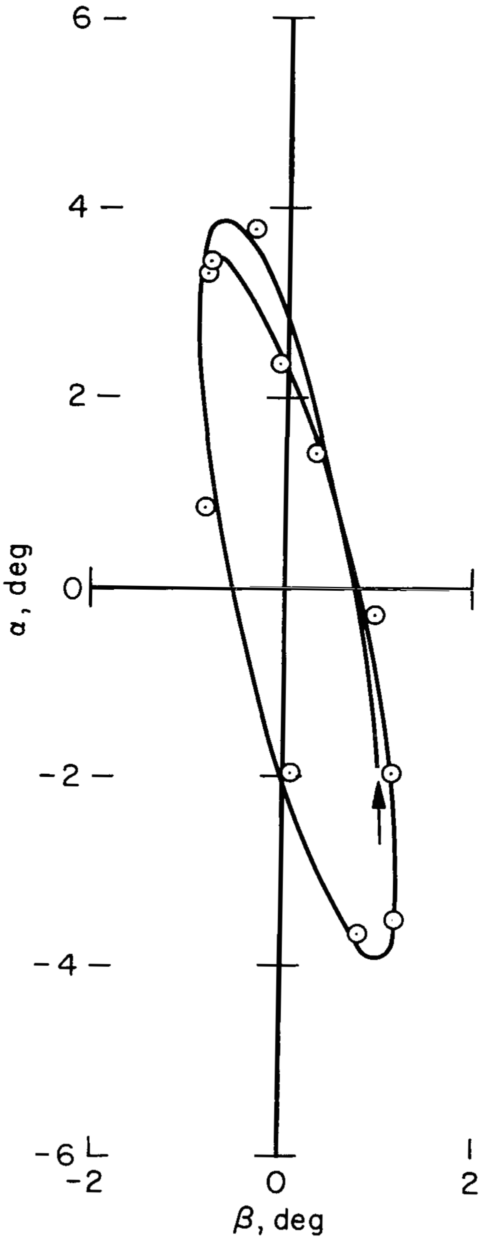

(e) Flight 987; M = 13.5

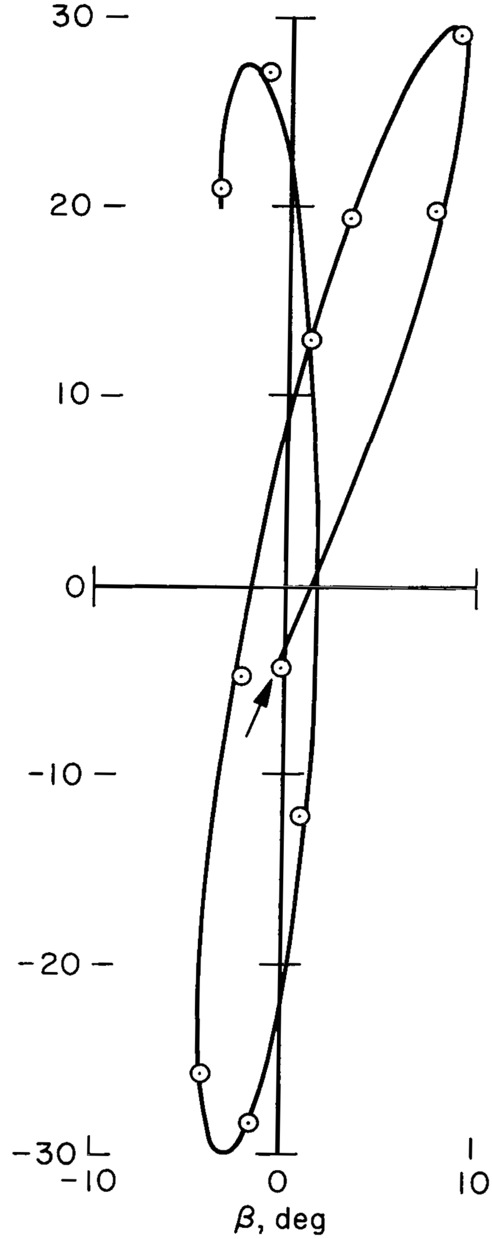

(f) Flight 985; M = 13.5

Figure 4.- Concluded.

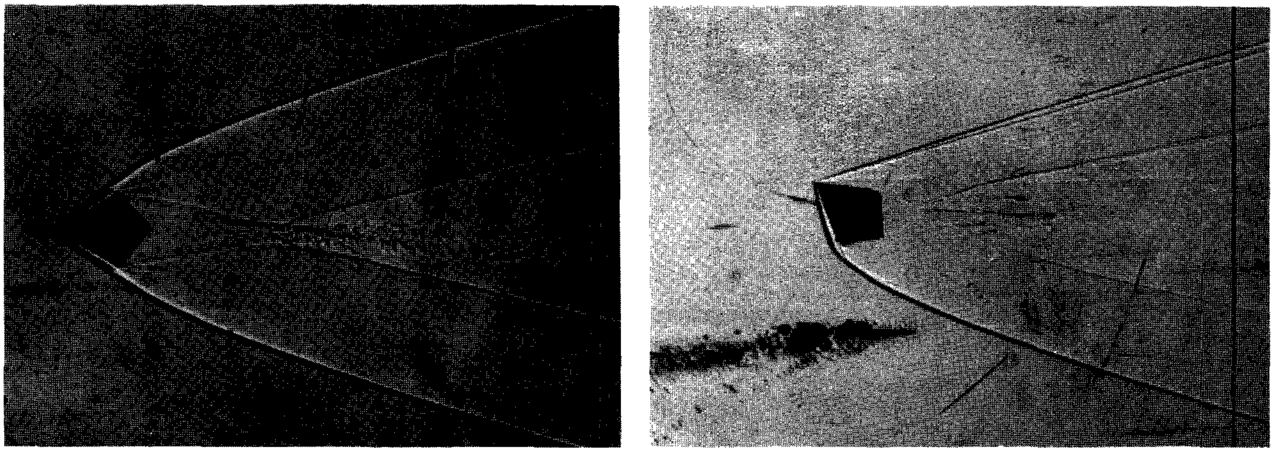

(a) M = 4.5

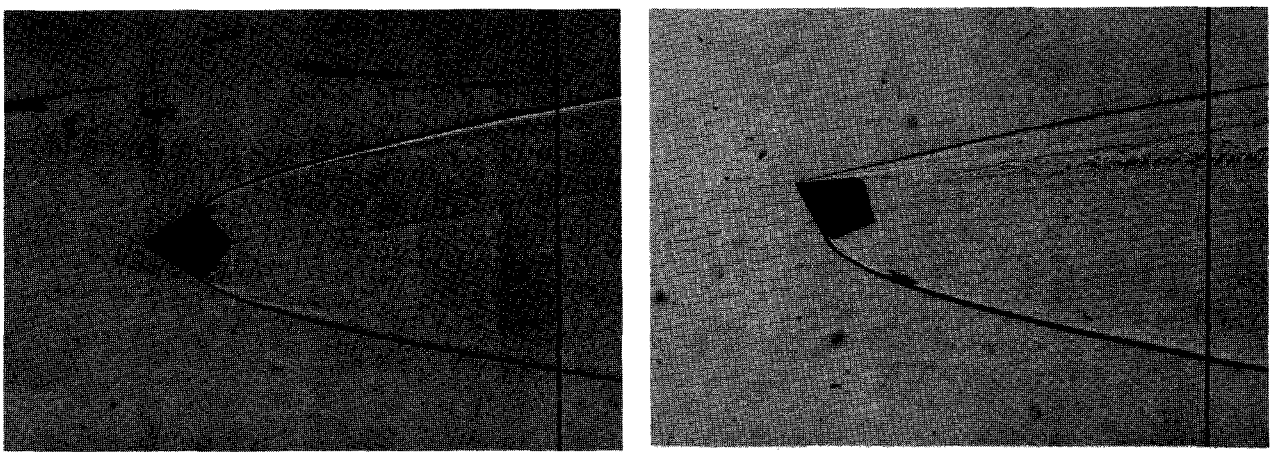

(b) M = 9.0

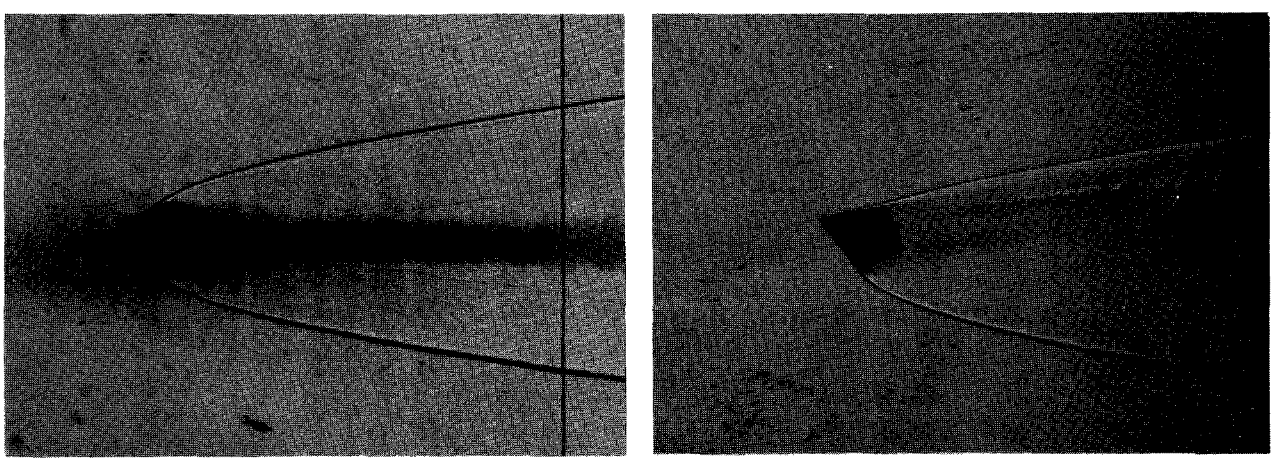

(c) M = 13.5

Figure 5.- Shadowgraphs showing flow-field phenomena of models flying in a 9-percent carbon dioxide, 91-percent nitrogen mixture.

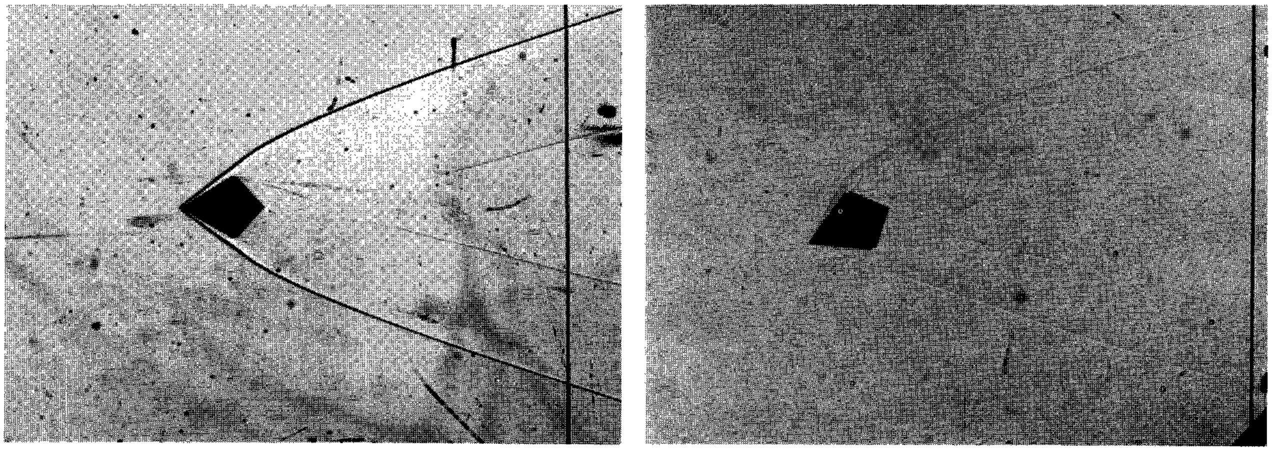

(a) M = 4.5

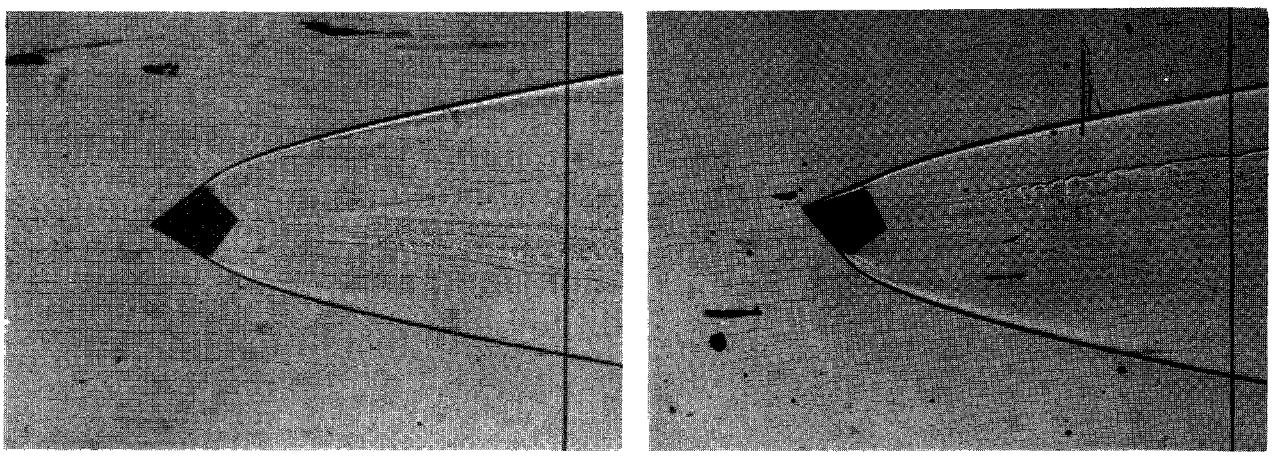

(b) M = 9.0

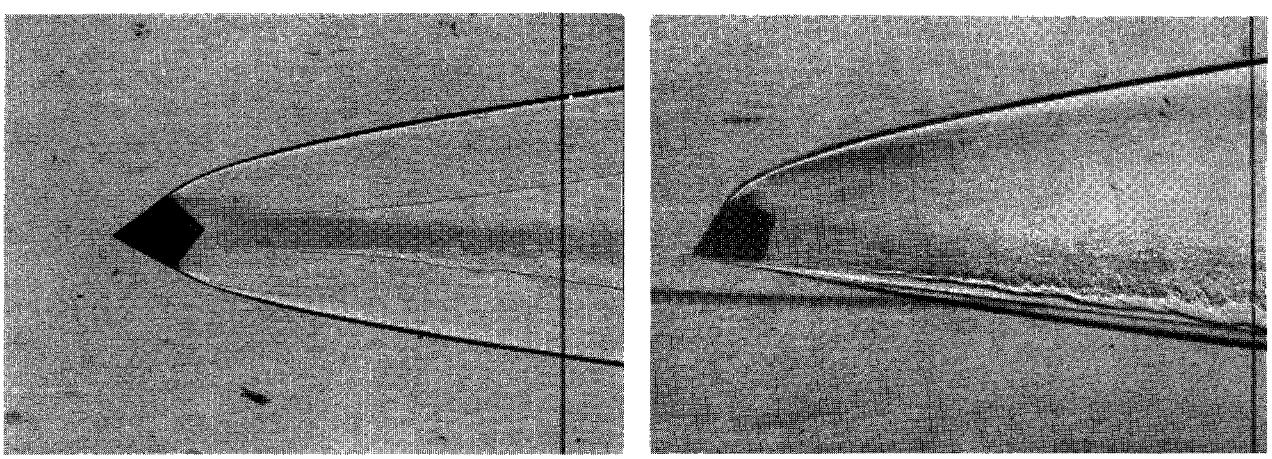

(c) M = 13.5

Figure 6.- Shadowgraphs showing flow-field phenomena of models flying in air.

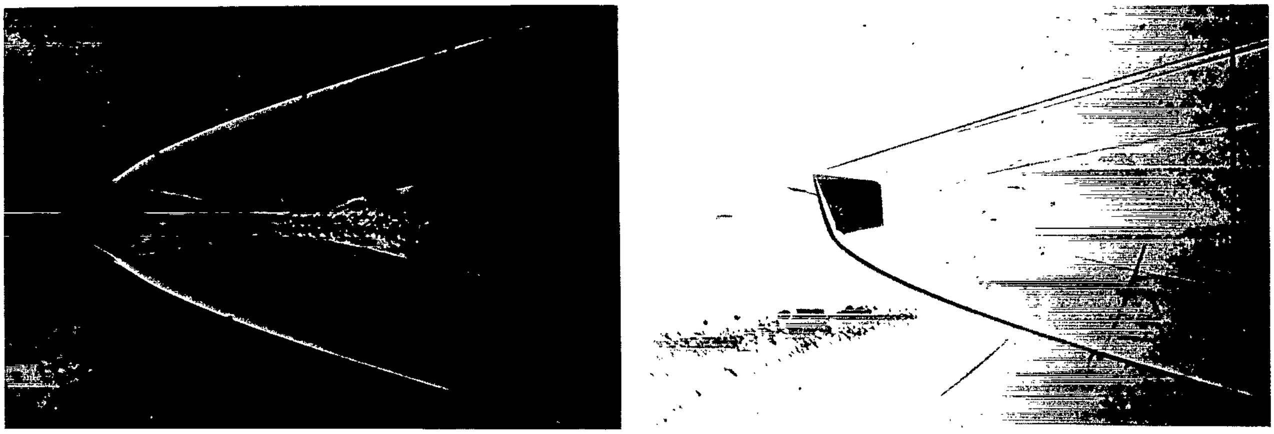

(a) M = 4.5

(b) M = 9.0

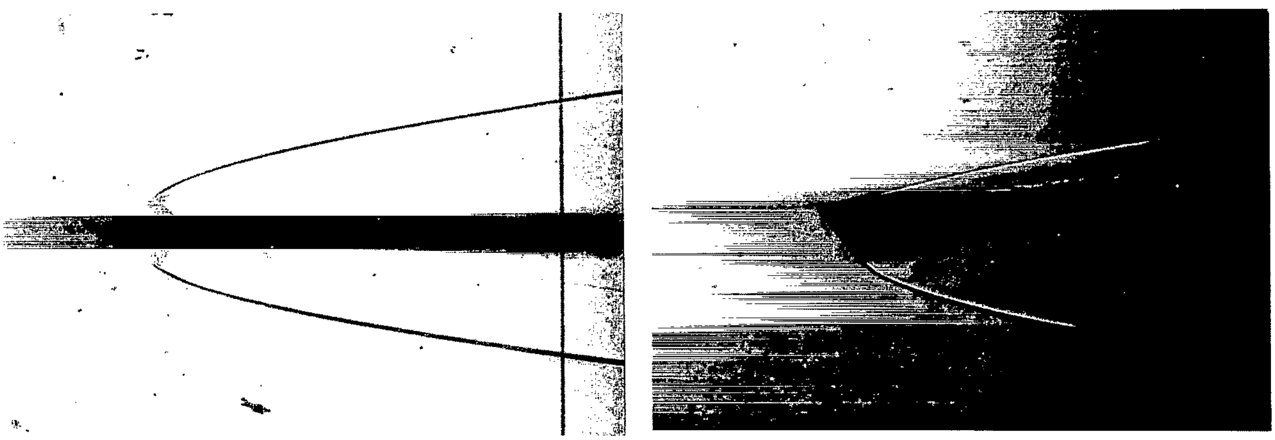

(c) M = 13.5

Figure 5.- Shadowgraphs showing flow-field phenomena of models flying in a 9-percent carbon dioxide, 91-percent nitrogen mixture.

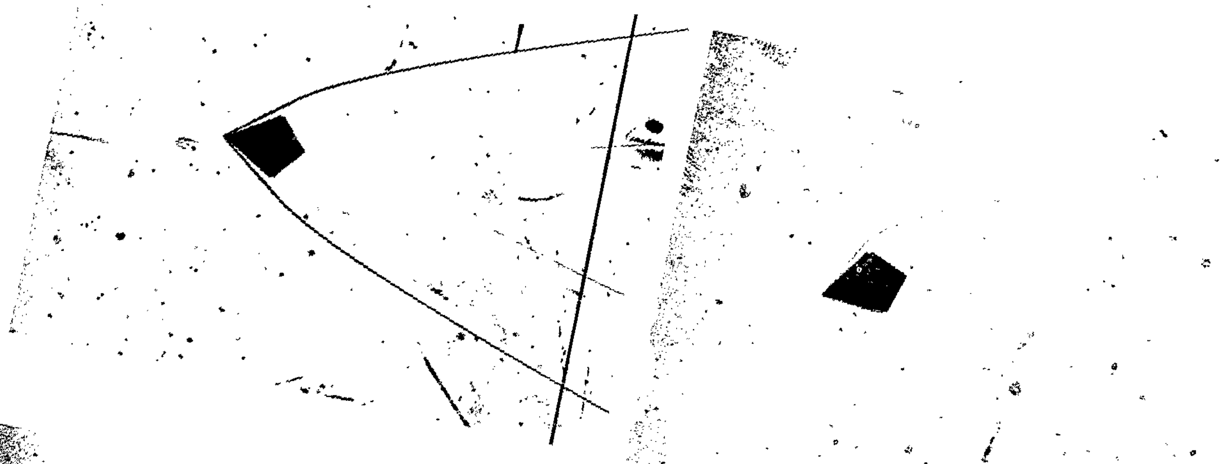

(a) $M = 4.5$

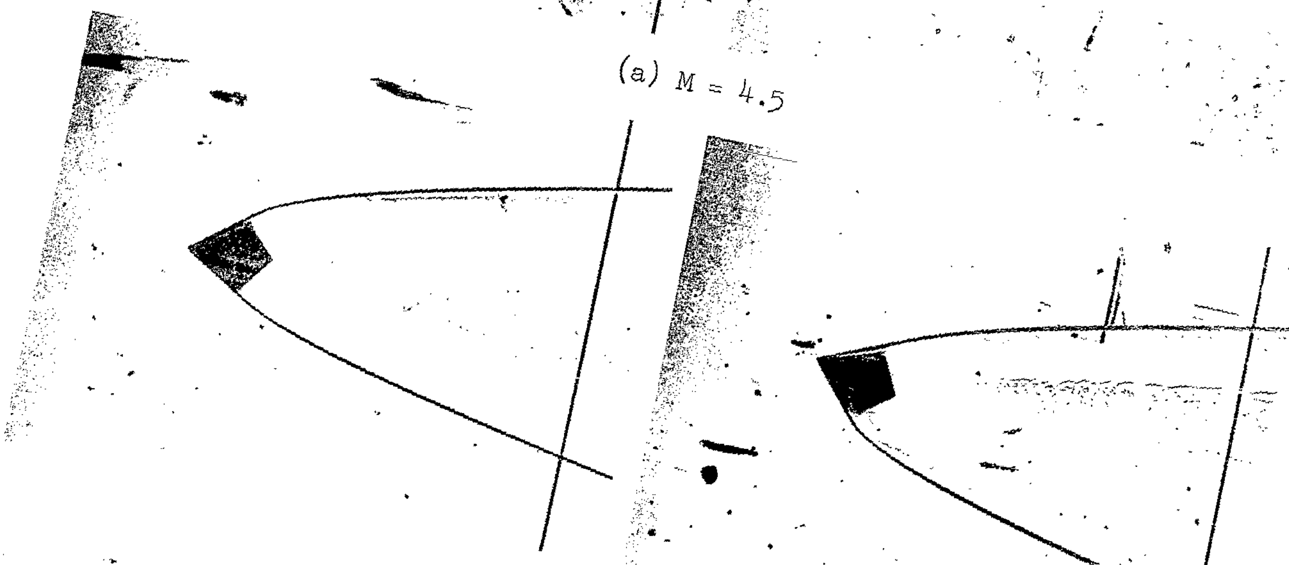

(b) $M = 9.0$

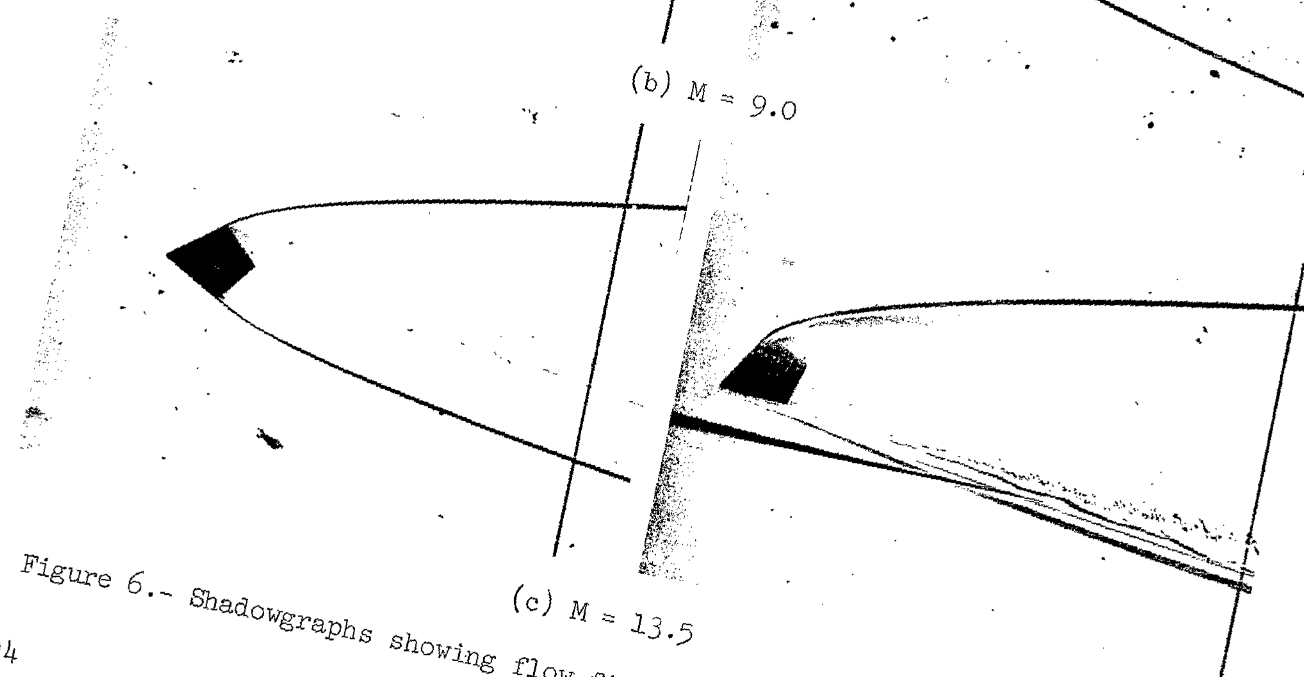

(c) $M = 13.5$

Figure 6.- Shadowgraphs showing flow-field phenomena of models flying in air.

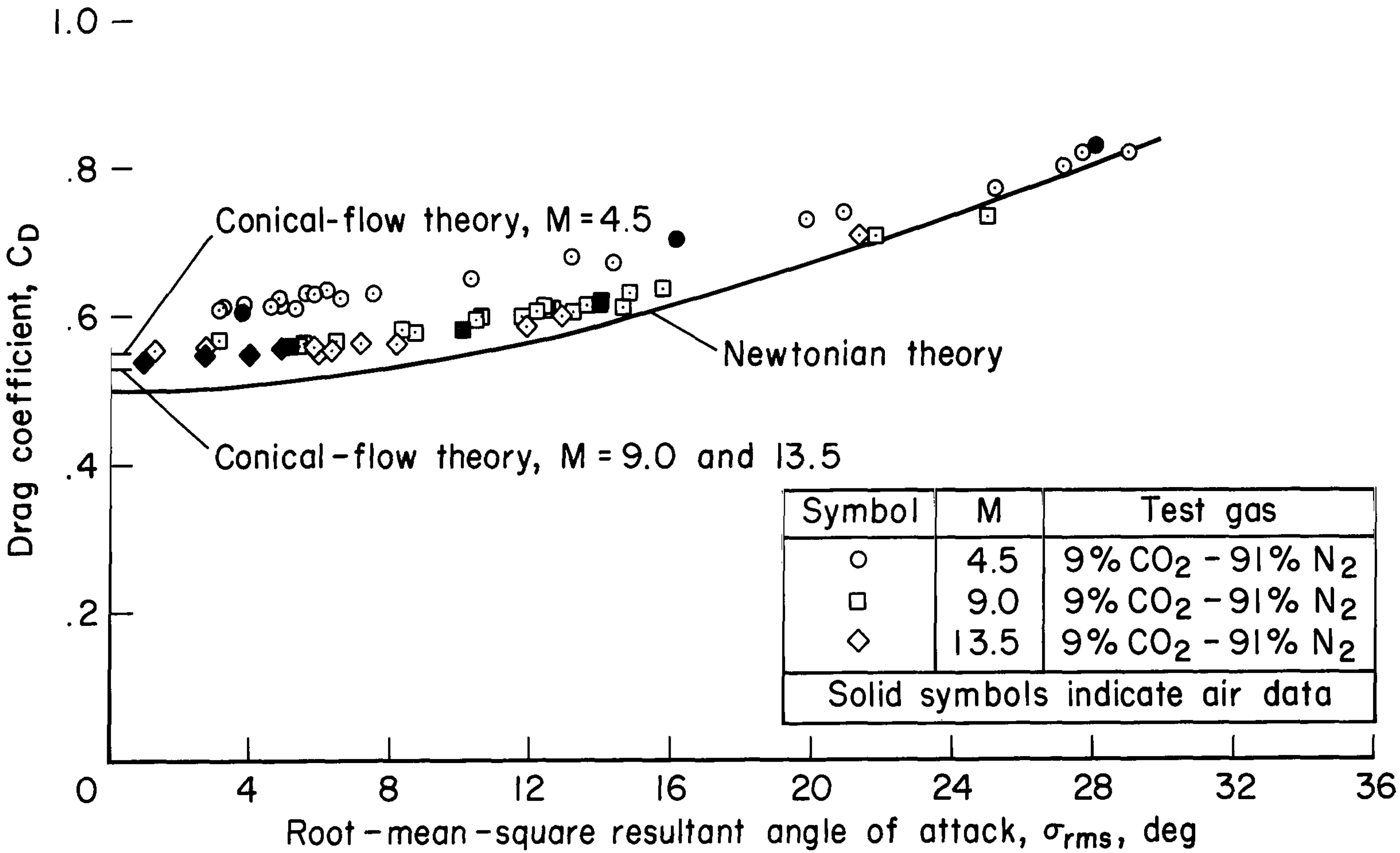

Figure 7.- Drag results.

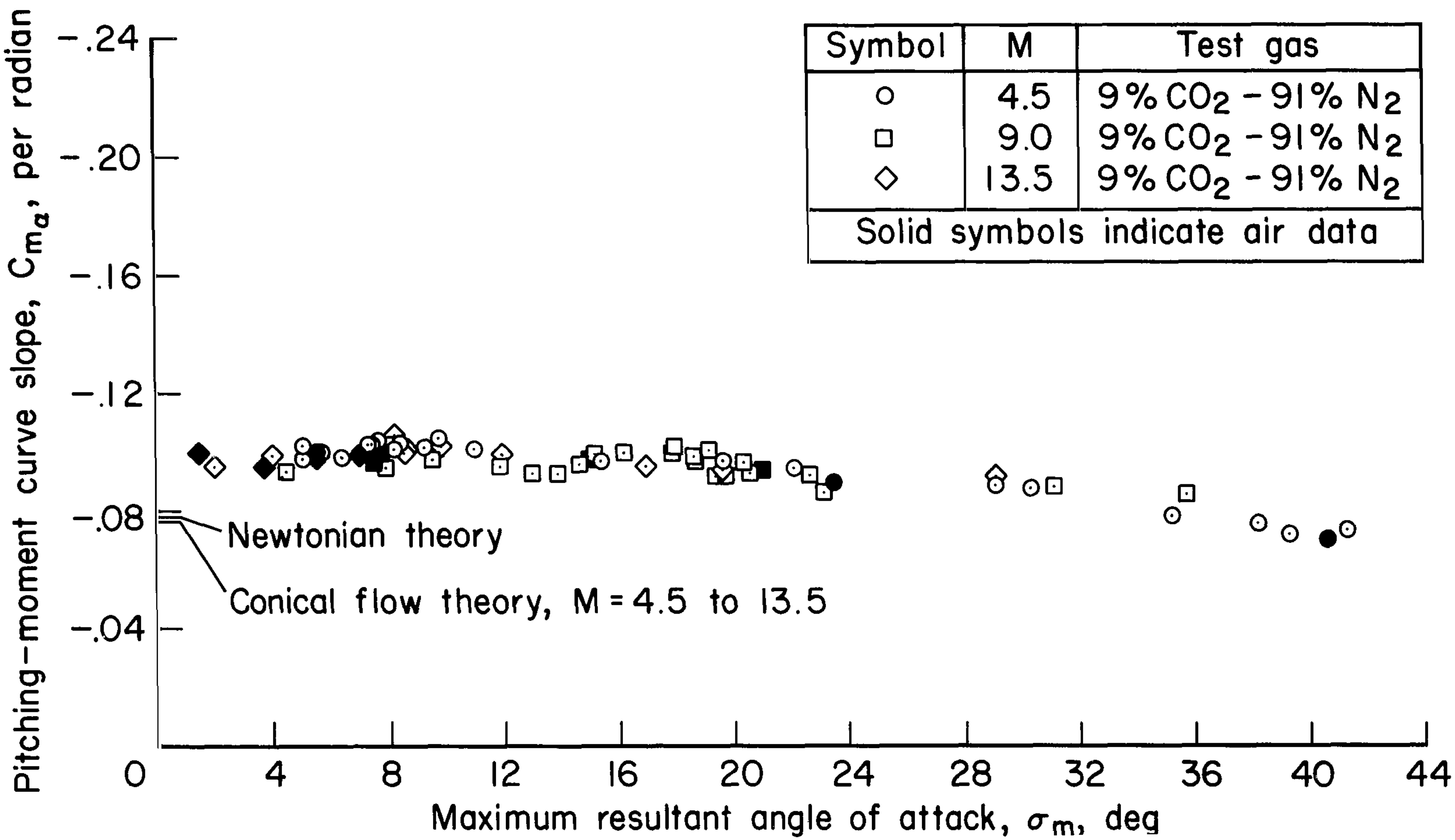

Figure 8.- Static stability results (linear analysis of data), $x_{cg}/d = 0.72$.

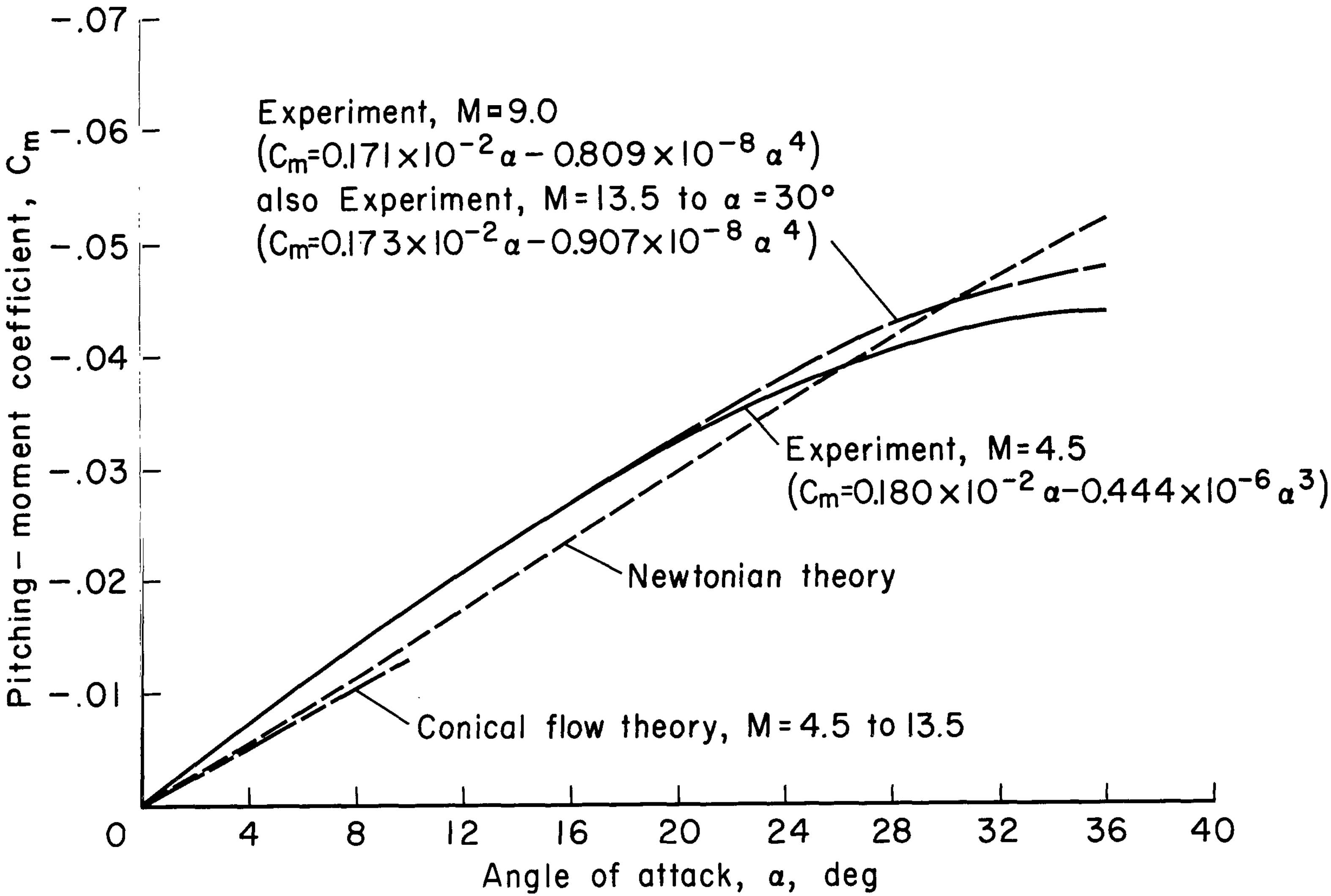

Figure 9.- Comparison of experimental pitching-moment coefficient with theory; $x_{cg}/d = 0.72$.

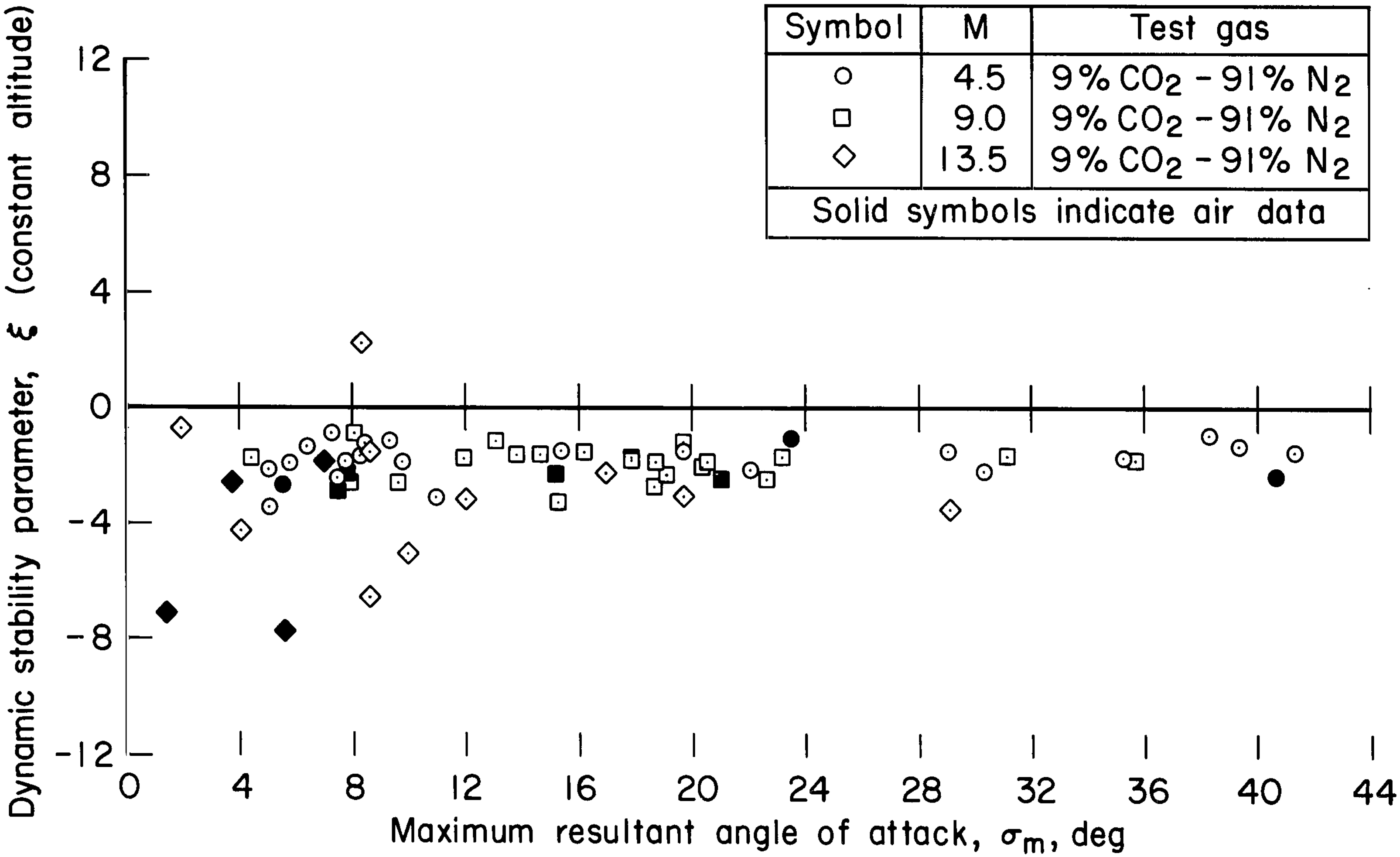

Figure 10.- Effects of Mach number and test gas on the dynamic stability parameter, ξ.

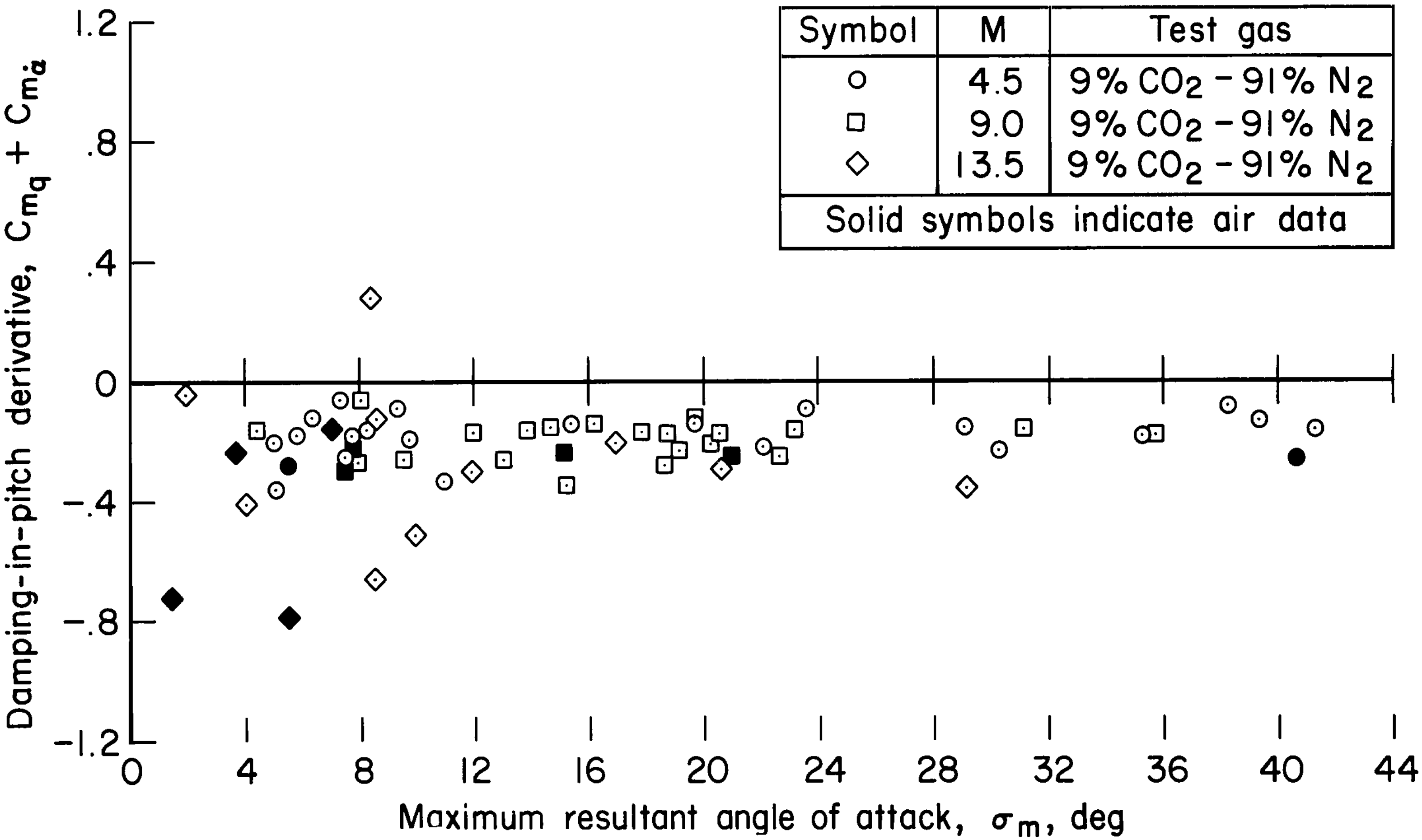

Figure 11.- Effects of Mach number and test gas on the damping-in-pitch derivative, $C_{m_q} + C_{m_{\dot{\alpha}}}$.

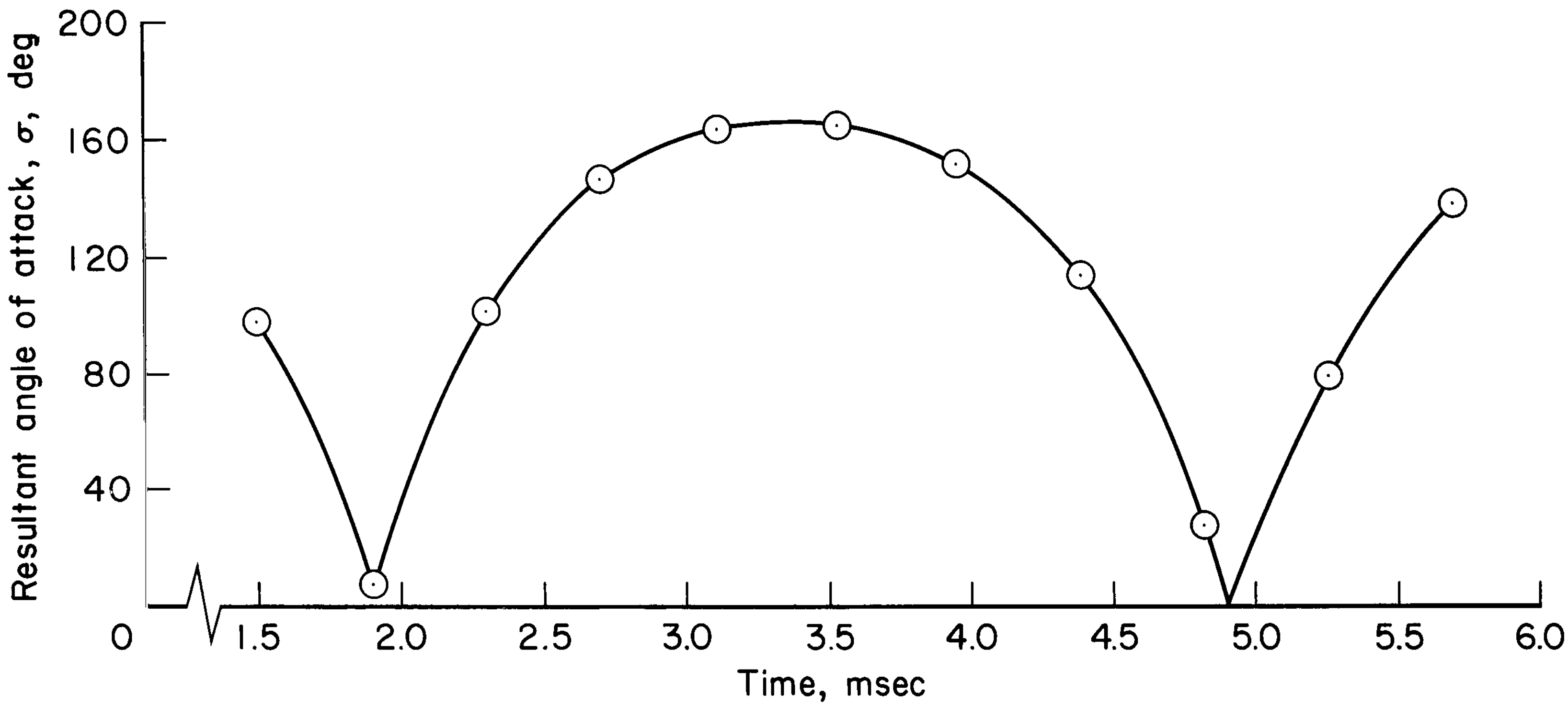

Figure 12.- Angular orientation time history of a model launched backward (flight 703); M = 8.36, Re = 0.72×10^6.

Symbol	Flight no.	Test gas	M range	Re range million	Facility
○	703	N_2-CO_2	9-8	.8-.7	Prototype hypervelocity free flight facility
●	663	Air	9-5	.8-.5	Pressurized ballistic range

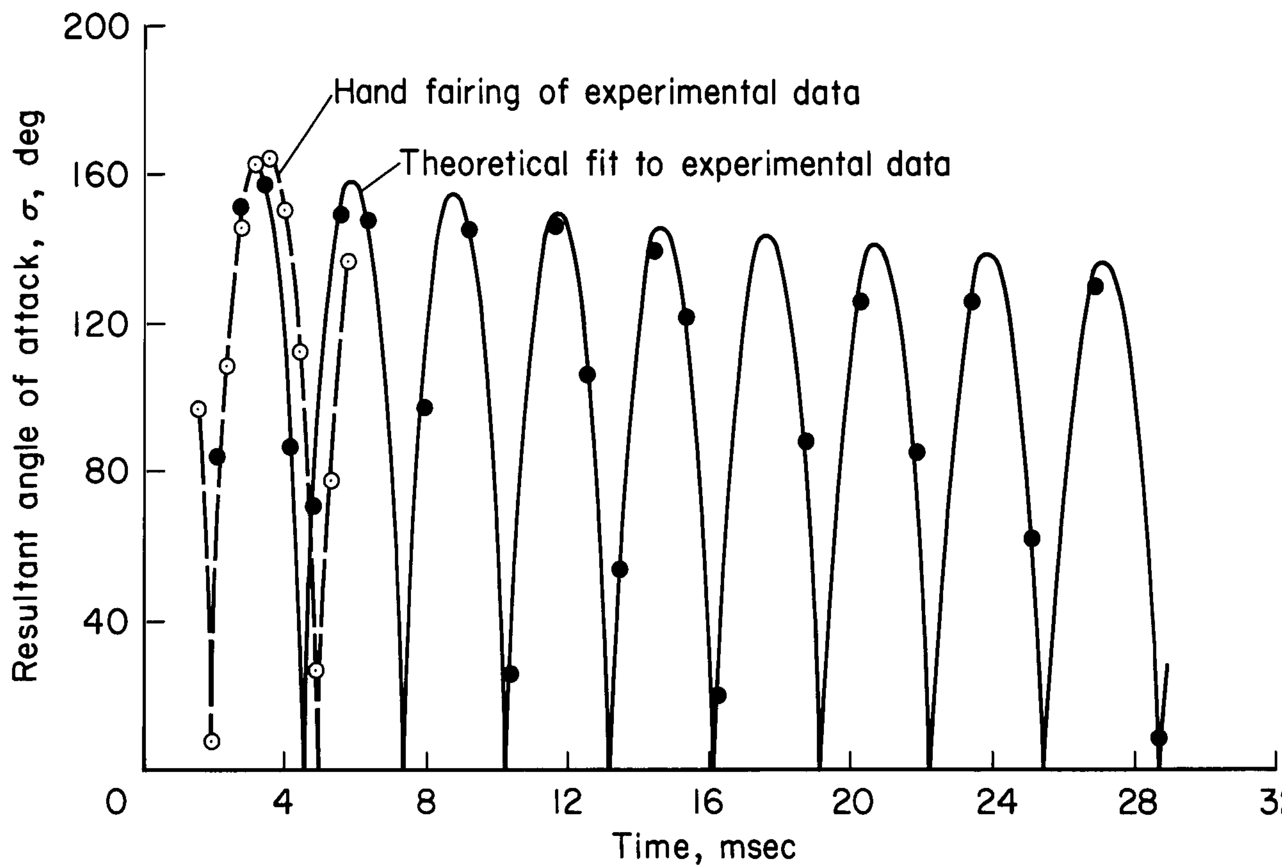

Figure 13.- Fit of theoretical motion equation (eq. (7)) to experimental data; $x_{cg}/d = 0.72$.

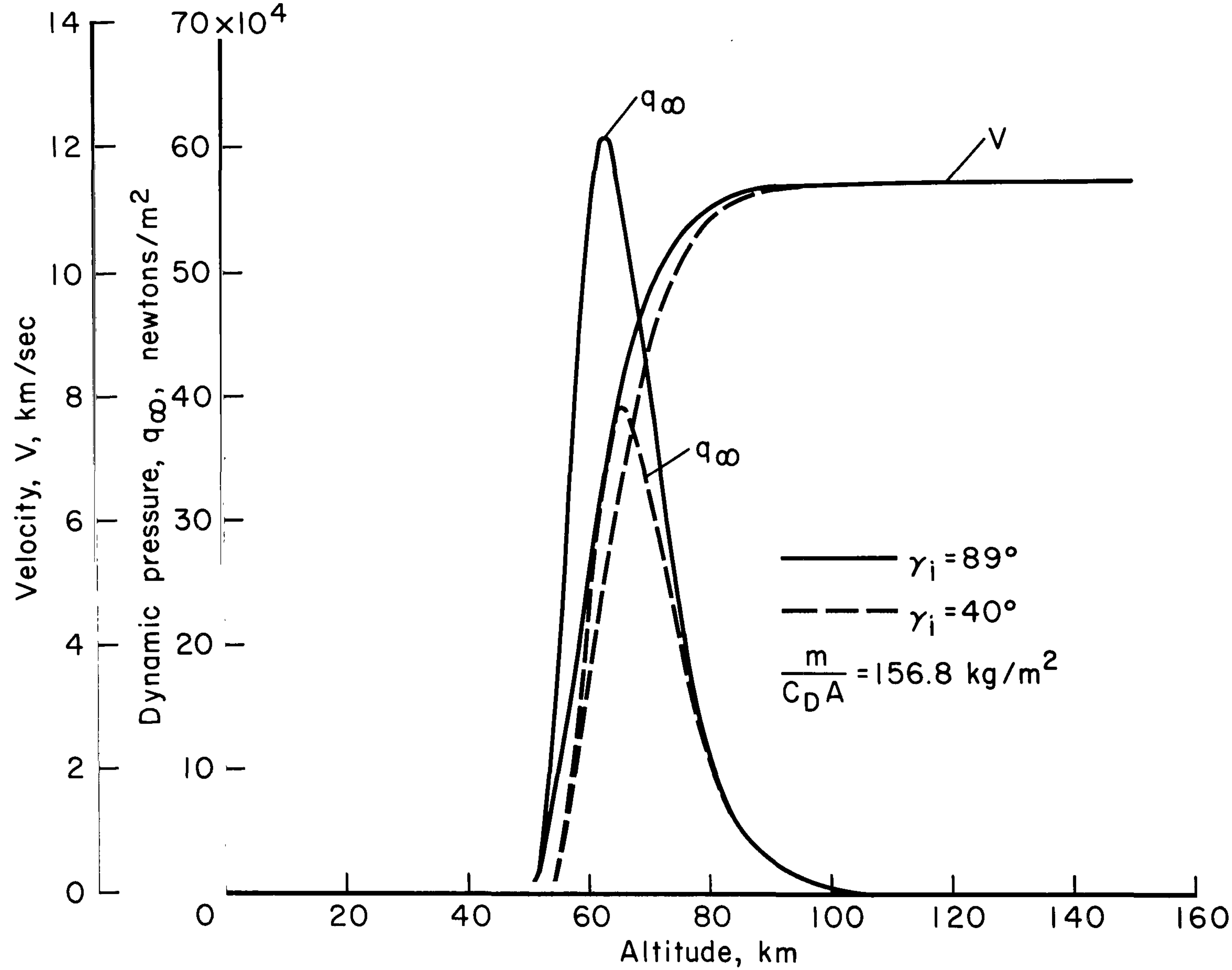

Figure 14.- Trajectory parameters related to motion of vehicle mass center.

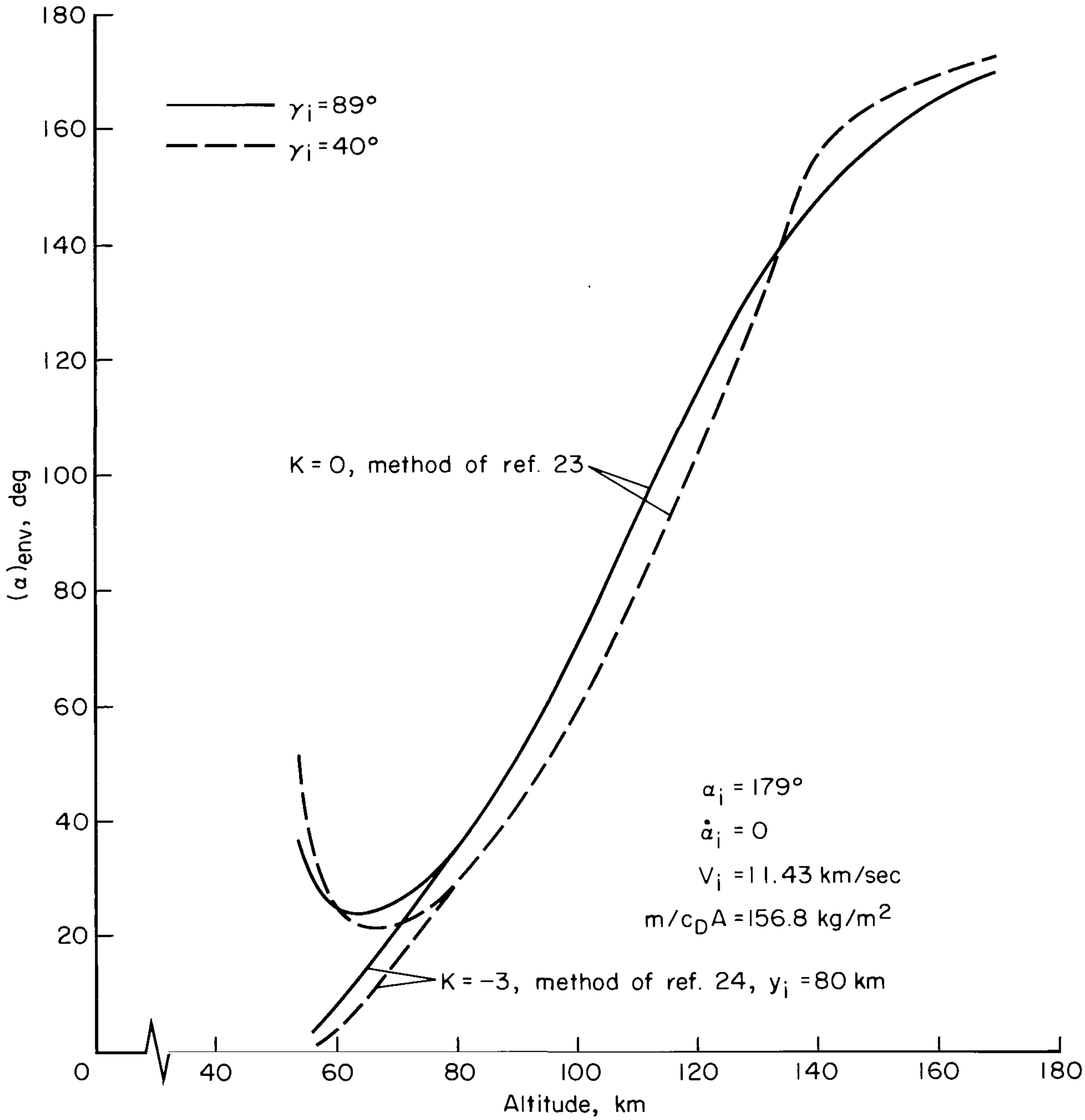

Figure 15.- Oscillation-amplitude histories of the configuration entering a model Venusian atmosphere.

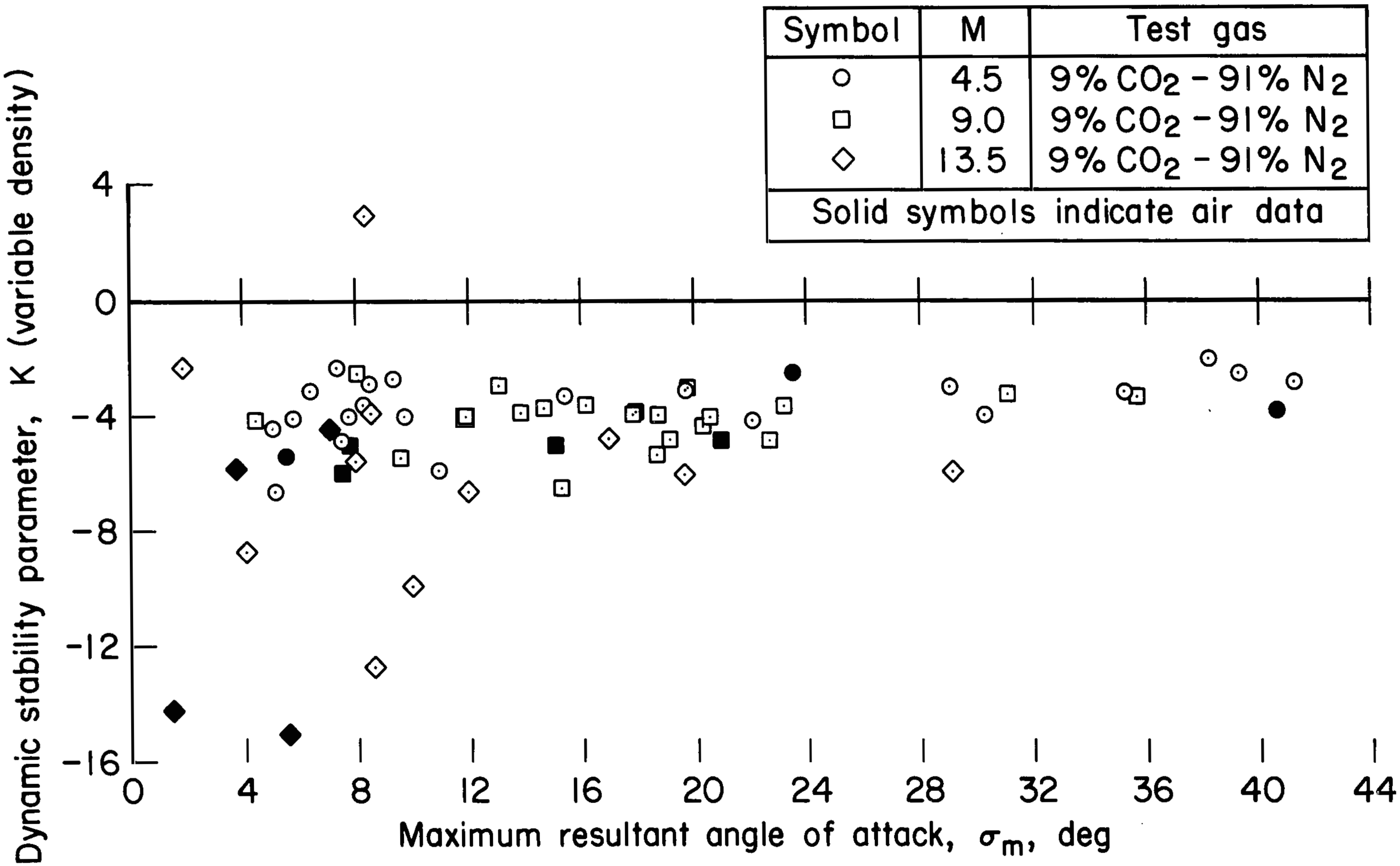

Figure 16.- Effects of Mach number and test gas on the dynamic stability parameter, K.

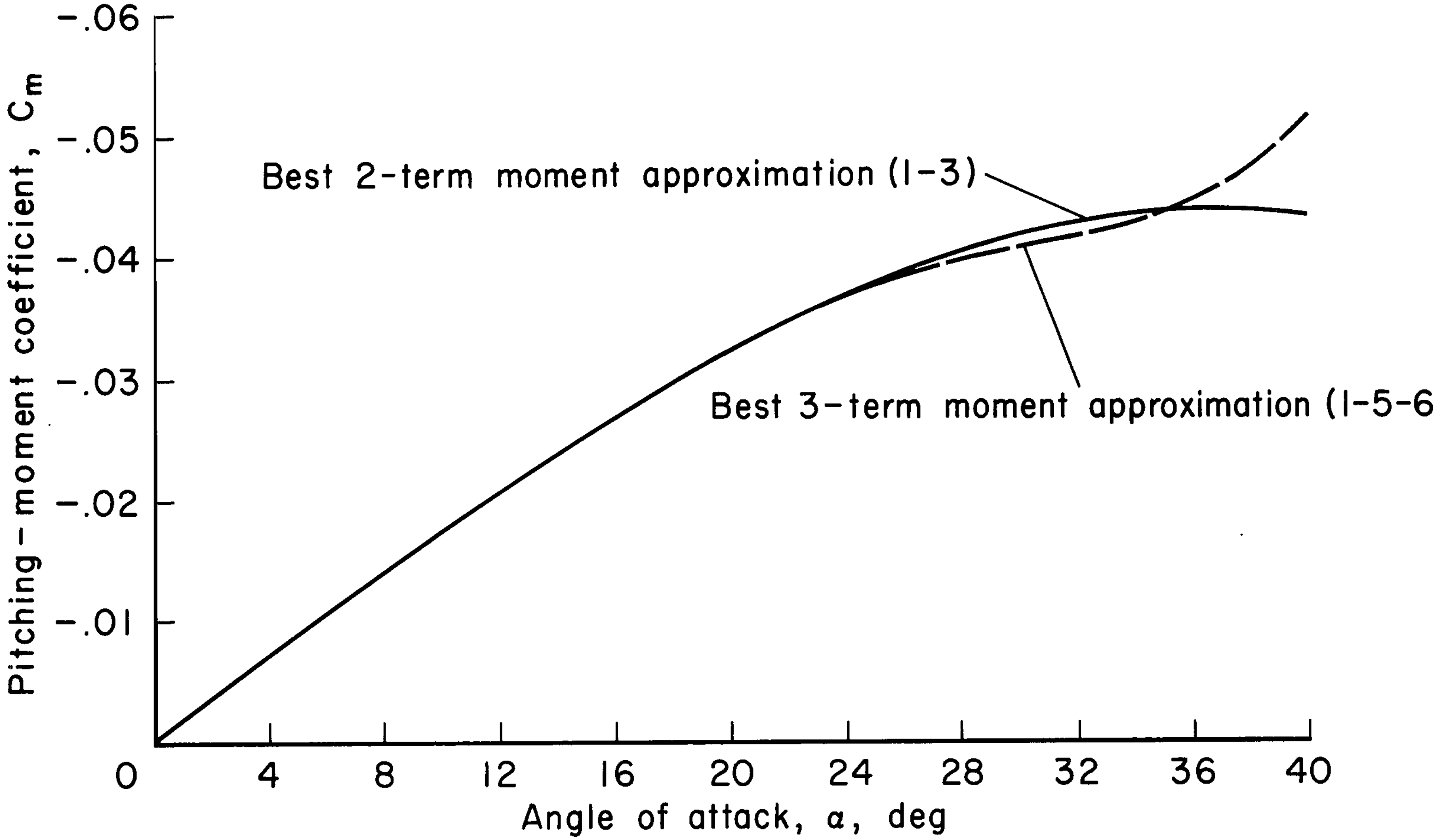

(a) M = 4.5

Figure 17.- Pitching-moment coefficient corresponding to the best 2- and 3-term assumed moment representations, x_{cg}/d = 0.72 d.

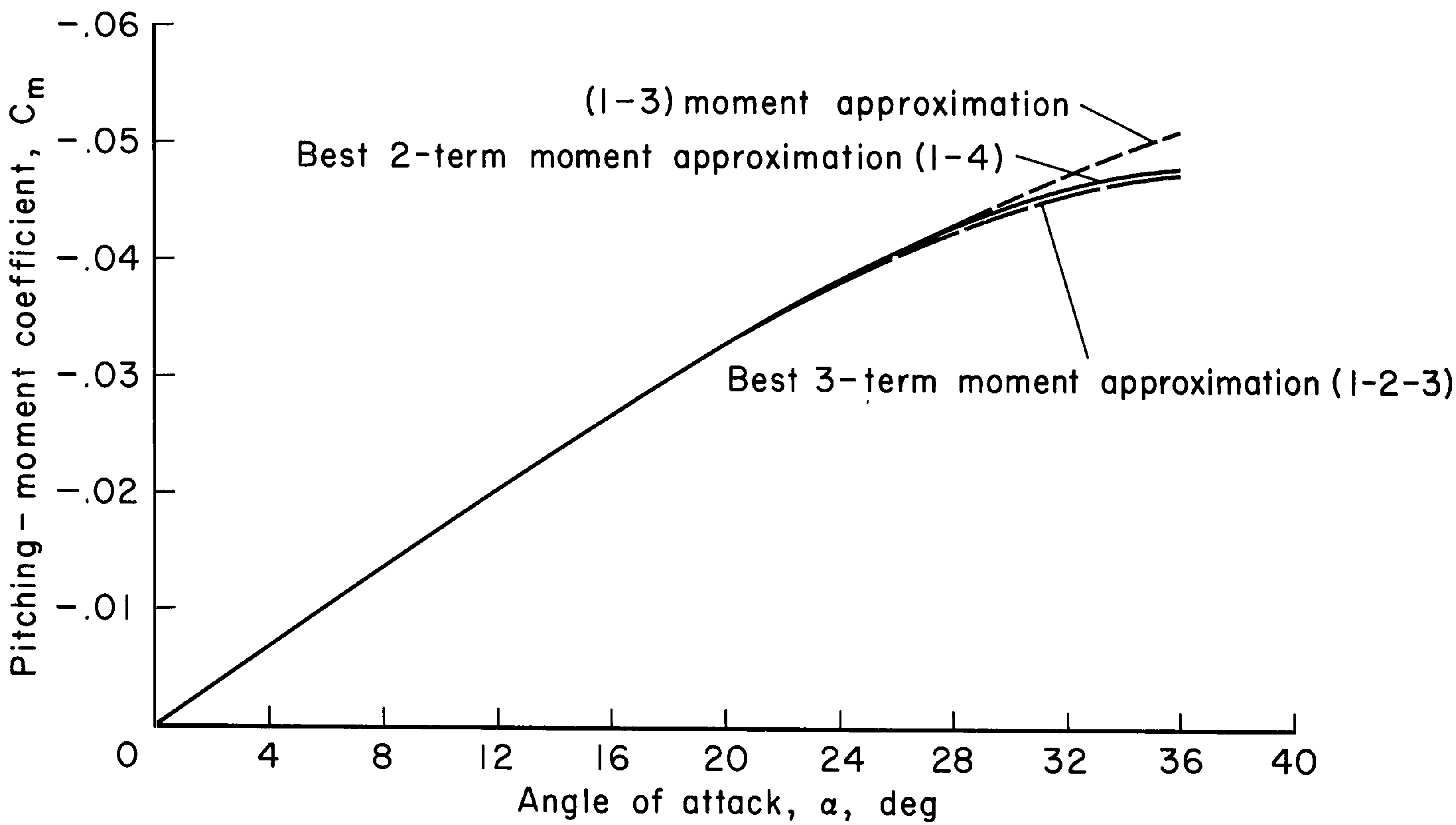

(b) M = 9.0

Figure 17.- Continued.

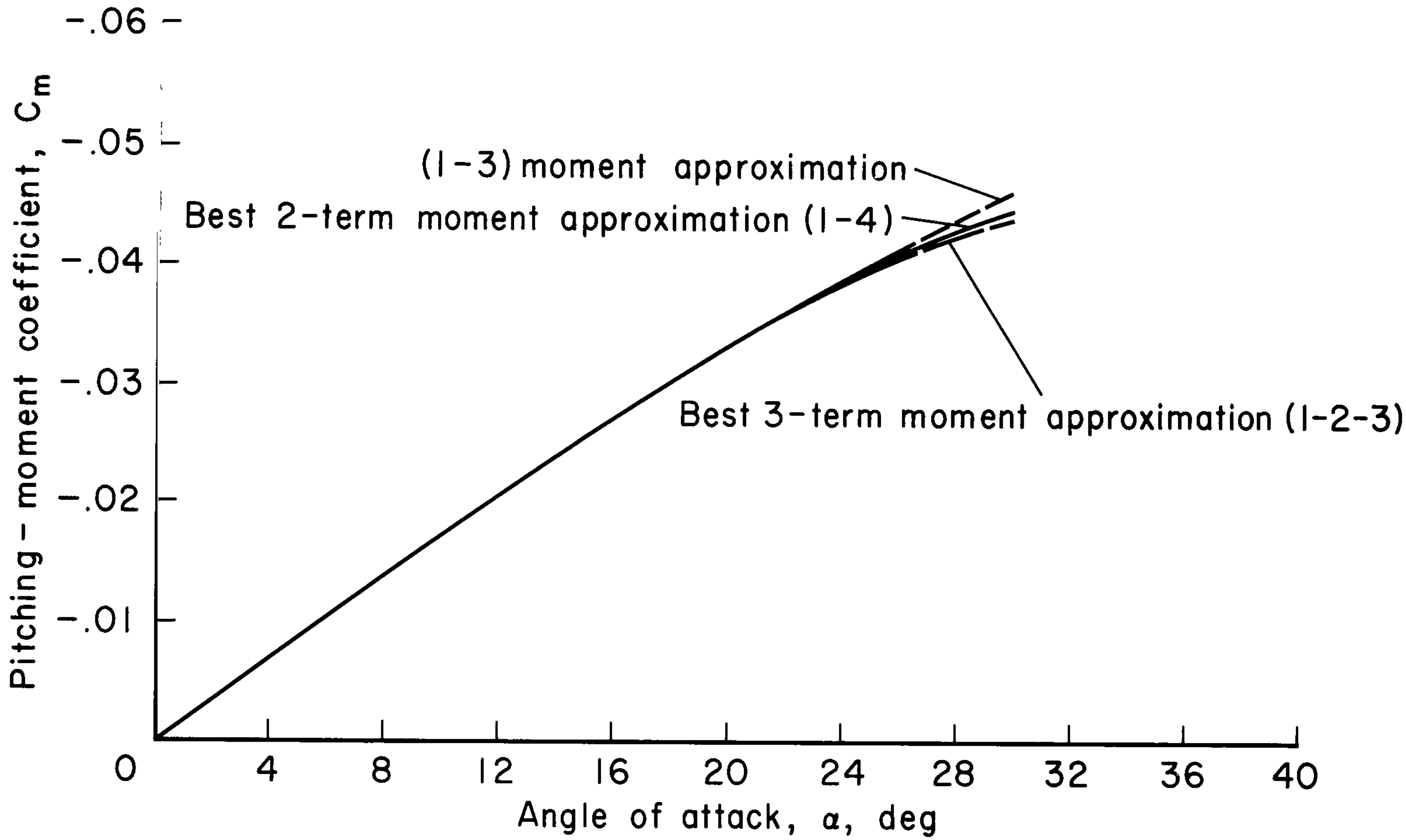

(c) M = 13.5

Figure 17.- Concluded.

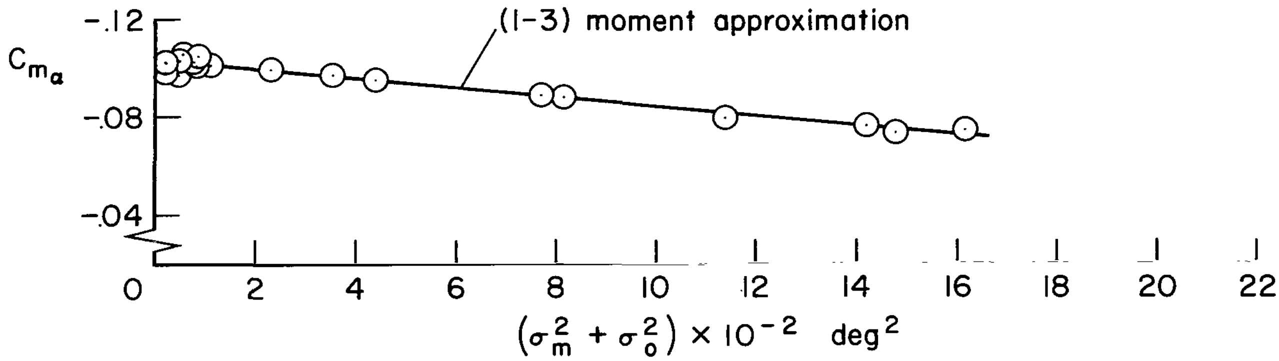

(a) M = 4.5

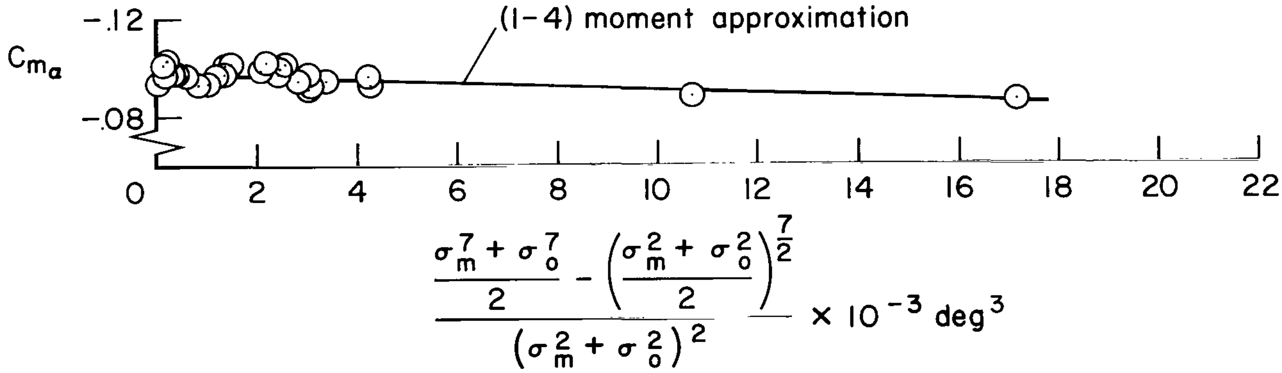

(b) M = 9.0

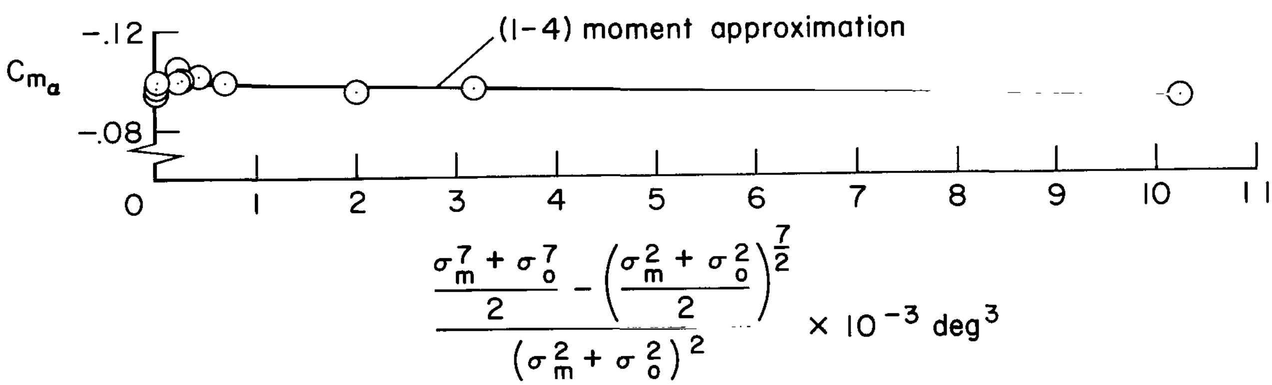

(c) M = 13.5

Figure 18.- Variations of C_{m_α} with amplitudes of the motion.

NASA-Langley, 1965 A-977

2/22/85

"The aeronautical and space activities of the United States shall be conducted so as to contribute . . . to the expansion of human knowledge of phenomena in the atmosphere and space. The Administration shall provide for the widest practicable and appropriate dissemination of information concerning its activities and the results thereof."

—NATIONAL AERONAUTICS AND SPACE ACT OF 1958

NASA SCIENTIFIC AND TECHNICAL PUBLICATIONS

TECHNICAL REPORTS: Scientific and technical information considered important, complete, and a lasting contribution to existing knowledge.

TECHNICAL NOTES: Information less broad in scope but nevertheless of importance as a contribution to existing knowledge.

TECHNICAL MEMORANDUMS: Information receiving limited distribution because of preliminary data, security classification, or other reasons.

CONTRACTOR REPORTS: Technical information generated in connection with a NASA contract or grant and released under NASA auspices.

TECHNICAL TRANSLATIONS: Information published in a foreign language considered to merit NASA distribution in English.

TECHNICAL REPRINTS: Information derived from NASA activities and initially published in the form of journal articles.

SPECIAL PUBLICATIONS: Information derived from or of value to NASA activities but not necessarily reporting the results of individual NASA-programmed scientific efforts. Publications include conference proceedings, monographs, data compilations, handbooks, sourcebooks, and special bibliographies.

Details on the availability of these publications may be obtained from:

SCIENTIFIC AND TECHNICAL INFORMATION DIVISION

NATIONAL AERONAUTICS AND SPACE ADMINISTRATION

Washington, D.C. 20546